Master Thesis at the
3D-Photovoltaics Group, AMOLF

Micro-confined ion transport in asymmetric Si-channels

Towards dynamic rectification of the ionic current

Author:

Blaise CUÉNOD

Supervised by:

Dr. Mark AARTS (AMOLF)

Dr. Esther ALARCÓN LLADÓ (AMOLF)

Prof. Anna FONTCUBERTA I MORRAL (EPFL)

Amsterdam, The Netherlands, March 2021
Master in Materials Science and Engineering at EPFL

Contents

1. Introduction

Inspired by the study of bio-channels present in living organisms, nano-fluidics, the study of ions and water transports in nano-scale structures, have been an active research field in the last two decades [1], [2]. In the case of nanopores or nanochannels, the ionic transport is mainly driven by the interactions of the ions with the surface and therefore significantly differs from the transport behaviour in the bulk. This influence of the interface between the electrolyte and the nanostructure can lead to interesting non-linear responses of the ionic fluxes to external stimuli such as pressure, potential or concentrations gradients [2], [3], [4]. From these non-linear responses, emerge various phenomena and applications such as ion-selective membranes [5], ionic diodes [6], [7], ionic transistors [8] or ion-pumps [9], [10].

Among these phenomena, the *ionic current rectification* (ICR) is one of the most studied. The ICR is characterized by a non-linear response of the ionic current through a nanochannel or pore to an applied external potential across the pore. The current response can be a diode-like response and therefore, exhibits a low and a high conductance state depending on the polarity of the potential applied. A particular application of the ICR is the blue or osmotic energy, in which the Gibbs free energy of mixing dissipated during the mixing of fresh water with the (salty)sea water is used for power generation. Theoretically, up to 0.8 kWh/m^3 could be harvested which is equivalent to the energy releases by water falling 270 m [11], [12]. Therefore, the mixing of the fresh water released in the sea by rivers represents a tremendous energy of 2 TW, from which 980 GW could be produced [13], [12], [14]. For comparison, 800 GW are estimated to be produced worldwide by hydropower such as dam and run-of-the-river power plants [13].

The main obstacle for the harvesting of this large and unused amount of energy, is the conversion efficiency of the processes used. Pressure-retarded osmosis (PRO) and reverse electrodialysis (RED) are seen to be the two most promising technologies among these processes. However, these two technologies do not show a sufficiently high conversion efficiency to be viable yet [11], [13]. Both of them are limited by the pores' sub-nano metric scales used within their membranes that lead to an high resistivity [11]. Alternatively, the ICR can be used in desalination processes using similar nano-porous membranes [9]. The efficiency of such membranes is therefore linked to two major challenges for society in the context of the climate change.

Siwy and Fulinski [10] have been among the firsts to use an ionic diode at nanometric scale and ICR to fabricate an ion pump. They use a conical pore etched into a 12 μm thick polyethylene terephthalate (PET) film. The conical pore reported has a 500 nm large opening diameter and a 2 nm small opening diameter. The pumping effect is reported coming from the combination of the ICR and the AC potential applied across the pore. They identified two main parameters related to pore itself influencing the rectifying properties, and consequently the pumping properties of the device. First, the inner pore walls have to be charged and second, the small opening needs to remain small enough ($\leq$ 15 nm). The rectifying phenomena is seen as a consequence of the Debye's layer overlap at the pore's tip and therefore a small opening is understood to be a prerequisite for ICR.

Several researches have been conducted on the influence of the nanochannels' surface charge density on the ICR. Lin et al. demonstrated the tunability of the rectification and the selectivity

of the nanopore with a kinetic functionalization of the inner surface of the channel [15]. The functionalization is done partially with poly-L-lysine on a 10 nm nanopore etched in PET membrane. This leads to an anion selectivity of the pore. In the order of the nA, the current behaviour of such channel showed a maximum rectification ratio, which is defined as the current ratio at opposite polarities of applied potential, (here at 1 V, $|I(+1V)/I(-1V)|$) of 60.

The asymmetrical modification of the surface charge density within the channel has been used to achieve rectification at the micrometre scale. Chang et al. used polyethyleneimine (PEI), a positively charge polyelectrolyte, and an anionic surfactant to modify the surface of one side of a micro biconical pore made of PET [16]. This leads to a positively charged surface on one side and a negatively charged one on the other side. He et al. also achieved rectification at micrometre scale by modifying micro-pipette inner surface with polyimidazolium brushes [17]. A maximum rectification ratio between 50 and 60 has been achieved. The achievement of rectification at micrometre scale, larger than the Debye ‘s length scale, has been attributed to the increased relative contribution of the surface conductance to the channel conductance.

The surface charge density having been identify as a key parameter for the ICR occurrence, its dynamic control could therefore lead to interesting applications in iontronics such as the ionic transistors. Kalman et al. demonstrated a single gated nanopore ionic diode [18]. The gating of the device has been achieved by depositing an insulated gold layer within the pore. A potential applied on this gold layer therefore modify the surface charge density of the pore and allows the tuning of the ICR occurrence. Other gate systems exist such as grafted polymer brushes whose swelling or expansion can be temperature-controlled or pH-controlled [19].

Two researches have recently demonstrated analytically that the ICR can be achieved at micrometres scale without chemical modifications of the surface charge density [2], [6]. They confirmed the role of the relative contribution of the surface charge as suggested in the reference [17] and they identify an asymmetric ion selectivity within the pore as a prerequisite for ICR.

Recent results within the group already proved experimentally this theory that ionic current rectification can be achieved with micrometre scale asymmetric channels without any chemical modifications. To the best of our knowledge, this is the first time such results are presented. This thesis aims to first confirm and complete these results and second to explore a potential dynamic modulation of the ionic current rectification phenomena. We investigate the conductance and the ICR behaviour of conical and straight microchannels fabricated by focused ion beam in a 2 µm thick silicon membrane with KCl electrolyte. The theoretical background used within the frame of this work is developed in the Chapter 2 where the electrical double layer model, the ionic current rectification and the conductance models for microchannels are explained. The Chapter 3 presents the experimental methods used to fabricate the micro-channels and to measure the conductance. The results are then presented in the Chapter 4 where the experimental conductances of the channels are compared to the theoretical model and where the role of the surface charge density on the current rectification is explained.

2. Theory

2.1. Solid-liquid interface model

The interaction at the interface between a solid charged surface and an ionic electrolyte has been first described by Helmholtz (1879) as a double layer composed of oppositely charged layers. The charge on the solid substrate is balanced by an accumulation of ions forming a monolayer close to the surface and form a simple capacitor [20]. The plane passing through the centre of the ions is now known as the Outer Helmholtz Plane (OHP) and the layer bound by the solid surface and this plane has been known as the Electrical Double Layer (EDL). However, this model does not account for the concentration dependency of the EDL capacity, the potential adsorption of ions on the surface and does not consider the ion diffusion away from the interface.

Gouy and Chapman later improved the model by seeing the EDL as a diffuse layer in which both counterions and co-ions are present; the former being attracted by the oppositely charged surface and the latter repelled, yielding a dynamic equilibrium of electrostatic attraction/repulsion and diffusion towards/away from the surface. Therefore, the charge distribution can be described by the Poisson-Boltzmann equations and (for low applied potentials, below the thermal voltage (Kb·T ~ 25mV)) leads to an exponentially decreasing charge distribution away from the surface.

The EDL commonly used nowadays has been suggested by Stern and is a combination of the Helmholtz and Gouy-Chapman models. For this model, the EDL therefore constitutes a layer of mainly counterions close to the surface, where the potential decays linearly from the electrode surface to the plane of closest approach, and a diffuse layer away from the surface, in which the potential decays exponentially with the distance[20][21]. Grahame further improves the model by proposing that specific adsorption of both counter,- and co-ions could occur at the surface, leading to a linear potential decrease/increase close to the surface before the decreasing potential regimes proposed by Stern [20].

The ion concentration, n_i, in the aforementioned diffuse layer can be described by:

$$n_i = n_i^o \cdot \exp\left(-\frac{z_i e\phi}{kT}\right) \tag{1}$$

Where the concentration in the bulk of ion i, n_i^o , is scaled by the Boltzmann distribution of the local electrostatic potential ϕ away from the surface, e is the elementary charge, z_i the charge of ion i, k the Boltzmann constant and T the temperature. The Poisson equation relates the spatial charge distribution q to the electrostatic potential along the channel length:

$$\nabla^2\phi(x) = -\frac{q(x)}{\epsilon_o\epsilon_r} \tag{2}$$

Combining Poisson's equation in 1D (equation 2) and the total charge density of all ionic species leads to the Poisson- Boltzmann equation and leads to:

$$\left(\frac{\partial \phi}{\partial x}\right)^2 = \frac{2kT}{\epsilon_r \epsilon_0} \cdot \sum_i n_i^0 \left[\exp\left(-\frac{z_i e \phi}{kT}\right) - 1\right] \tag{3}$$

In the case of a dilute symmetric 1:1 electrolyte such as KCl, the latter equation can be written as:

$$\frac{\partial \phi}{\partial x} = -\left(\frac{8kTn^0}{\epsilon_r \epsilon_0}\right)^{\frac{1}{2}} \cdot \sinh\left(\frac{ze\phi}{2kT}\right) \tag{4}$$

Which can be written as:

$$\int_{\phi_0}^{\phi} \frac{d\phi}{\sinh\left(\frac{ze\phi}{2kT}\right)} = -\left(\frac{8kTn^0}{\epsilon_r \epsilon_0}\right)^{\frac{1}{2}} \int_0^x dx \tag{5}$$

The integration of equation (5) further leads to:

$$\frac{\tanh\left(\frac{ze\phi}{4kT}\right)}{\tanh\left(\frac{ze\phi_0}{4kT}\right)} = e^{-\kappa x} \tag{6}$$

Where $1/\kappa$ is defined as the characteristic distance λ_D, known as the Debye's length:

$$\lambda_D = \sqrt{\frac{\epsilon_r \epsilon_0 kT}{2n^0 z^2 e^2}} = \sqrt{\frac{\epsilon_r \epsilon_0 kT}{2cN_A z^2 e^2}} \tag{5}$$

Where c is the concentration, N_A the Avogadro's number and $\epsilon_r \epsilon_0$ is the permittivity of the solution. The overlap of the EDL within nanoscale channels has been thought to be a prerequisite to achieve ionic current rectification (ICR) due the selective properties of the interface region, [5]. Therefore, the Debye length has been the characteristic length that would limit the channel size and geometry.

It has been shown recently that ICR can be achieved in larger systems in the microscale, therefore larger than the EDL thickness, by increasing the charge density on the pore's inner surface [17][22]. It suggests that the surface charge density plays a key role in the ICR occurrence rather than the relative thickness of the Debye layer to the pore radius. Poggioli et al.[2] demonstrated that the ICR occurrence in asymmetric microscale channels can be predicted by the relative magnitudes of the surface and bulk conductance, as described by the so-called Dukhin length l_{Du} [1][6]:

$$l_{Du} = \frac{|\sigma|}{e \cdot c_{bulk}} \tag{6}$$

Where σ is the surface charge density, e the elementary charge and c_{bulk} the bulk concentration. l_{Du} describes the length at which the surface conductivity is comparable to the bulk conductivity and can be rewritten as a dimensionless number, the so-called Dukhin number Du when normalized by the channel radius R :

$$Du = \frac{l_{Du}}{R} = \frac{|\sigma|}{e \cdot c_{bulk} \cdot R} \tag{7}$$

Therefore, from equation (7), a Dukhin number larger than 1 indicates a dominant surface conductivity over that of the bulk. Figure 1 shows the evolution of the Debye length for KCl as function of its concentration. The thickness of the EDL therefore range from tens of nanometres at 0.1 mM to less than one nanometres at 0.1 M. The Dukhin length for a radius of 1µm and surface charge of 100 mC/m^2 is also shown. It ranges from 10 µm at 10^{-4} M to 10 nm at 0.1 M.

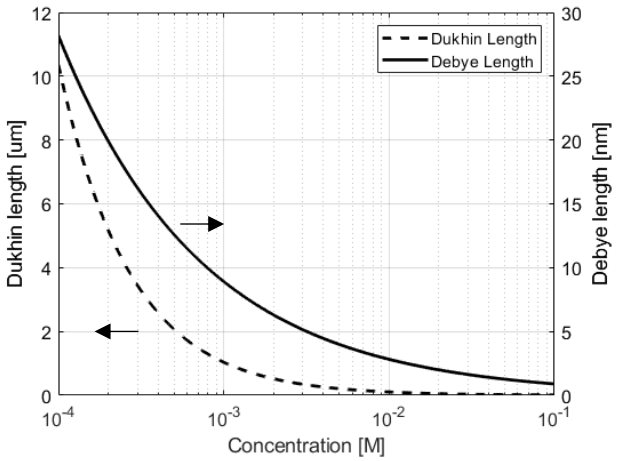

Figure 1: Debye length as function of the KCl concentration at 300 K with ϵ_r= 67 using the equation (5). The Dukhin length is calculated for a radius of 1 um and a surface charge of 100 mC/m^2 using the equation (6).

2.2. Transport phenomenon near interfaces

In small confined fluidics systems such as nanochannels, the ionic transport is strongly influenced by the interfaces between the substrate and the electrolyte. As shown in section 2.1, the ion distribution in the EDL close to the surface is not homogeneous and leads to non-neutral charge within the layer, as the surface charge density present on the substrate attracts the counter-ions and repels the co-ions. This exclusion of co-ions close to the surface therefore makes the ionic transport selective for the polarity of ionic charge within the double layer, [5].

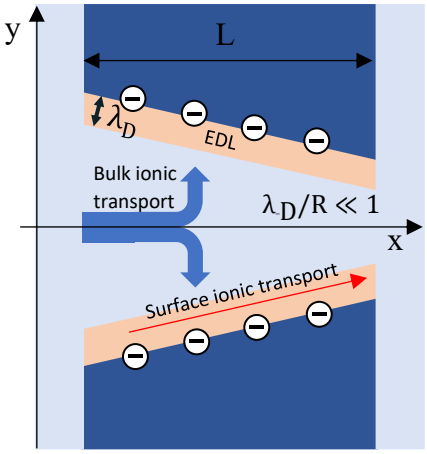

Figure 2: Schematic of a tapered channel (dark blue). The EDL is depicted in red. The electrolyte concentration is the same on both sides of the channel.

As mentioned in the previous section, a Dukhin number above 1 indicates a dominant surface conductance over that of the bulk. Consequently, it also indicates at which dimensions the charge-

selective transport starts to dominate. Figure 2 depicts the case of a geometrically asymmetric tapered channel. The varying channel width therefore leads to a varying local Dukhin number along the channel length.

Let's assume that the large opening (base) on the left-hand side of the channel is characterized by $Du \ll 1$ and that the small opening (tip) by $Du \approx 1$. Furthermore, the electrolyte is assumed to be symmetrical 1:1, with all ions having the same mobility. Under an applied electric field across the channel, from base to tip, the ionic transport on the base side is mainly controlled by the bulk response. Therefore, the counter-ions and the co-ions have an equal relative contribution to the total ionic current at the base. On the tip side, due to the dominant selective transport, the counter-ions have a larger relative contribution to total current. As the total current has to be constant along the channel's length, the asymmetry in ion selectivity leads to a depletion of the ions within the channel, lowering its overall conductance (low conductance state). In the case of an electric field applied from tip to base, this asymmetric selectivity leads to an accumulation of ions within the channels, increasing the overall conductance (high conductance state) [6]. This asymmetry in selectivity results from the geometric asymmetry of the channel but can also result from an asymmetry in the surface charge density [2], [16] or from an asymmetry in the concentrations between both sides of the channel. [2].

Dal Cengio et al. [6] have shown that the ion selectivity of a certain ionic specie ($c_{+,-}$) along the channel can be expressed as the ratio of its local concentration over the sum of the local concentration of all ionic species present. This selectivity γ, here below for the counter-ion, can be further expressed as function of a reference Dukhin number, defined as the Dukhin number halfway through the channel [6]:

$$Du_{ref} = \frac{|\sigma|}{e \cdot c_{bulk} \cdot R_{ref}} = \frac{|\sigma|}{e \cdot c_{bulk} \cdot \frac{R_{base} + R_{tip}}{2}} \tag{8}$$

$$\gamma_+^{Base} = \frac{c_+^{Base}}{c_+^{Base} + c_-^{Base}} = \frac{\left(\frac{Du}{R_{Base}} + \sqrt{\left(\frac{Du}{R_{Base}}\right)^2 + 1} \right)}{2\sqrt{\left(\frac{Du}{R_{Base}}\right)^2 + 1}} \tag{10}$$

$$\gamma_+^{Tip} = \frac{c_+^{Tip}}{c_+^{Tip} + c_-^{Tip}} = \frac{\left(\frac{Du}{R_{Tip}} + \sqrt{\left(\frac{Du}{R_{Tip}}\right)^2 + 1} \right)}{2\sqrt{\left(\frac{Du}{R_{Tip}}\right)^2 + 1}} \tag{11}$$

Therefore, for the symmetric 1:1 electrolyte, the selectivity ranges from 0.5 (non-selective) to 1 (perfectly selective). Figure 3 shows the selectivity as function of the bulk concentration. It is apparent that the transition from the non-selective to the perfectly selective regimes on the tip side does not appear within the same concentration range as the base side. The difference between the two selectivities, depicted by the blue area, therefore reaches a maximum at certain concentration, or alternatively at certain reference Du (the Dukhin number halfway through the channel). This maximum can be seen as the point where the conditions within the tapered channel lead to the highest asymmetry between the low and high conductance states mentioned above.

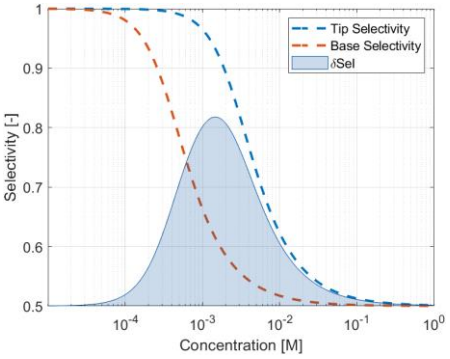

Figure 3: Example of the selectivity model of Dal Cengio. In blue, the selectivity at the tip, in red at the base. The blue shaded area depicts the difference between the two selectivities.

This asymmetry in the ionic conductance between a negative and a positive potential is known as the ionic current rectification (ICR)[1], [2], [6].

The ICR is defined in the literature as the ratio of the absolute current of the two opposite polarities [2], [6]:

$$ICR = \frac{|I(-V)|}{|I(+V)|} \tag{12}$$

In this work, assuming that the high and low conductance states at opposite polarities are both ohmic, we defined the ICR as the ratio of the average of the differential conductance between (+/) 0.25 V and (+/-) 0.5 V. This choice of using an average of the differential conductance allows us to limit the influence of parasitic noises appearing during the measurements. The potential range chosen is justified by the presence of leakage current which is further explained in section 4.2.

In summary, the selectivity is governed by the relative contribution of the surface conductance to the bulk conductance. The Dukhin's length and number are the key metrics to define this relative contribution and therefore lead to selectivity at larger scale within the micron range. The ionic current rectification phenomena derived from an asymmetry of this selectivity along the channel length. This asymmetry in selectivity can be the result of a geometrical asymmetry as explained above or alternatively of an asymmetry in the surface charge density within the channels (charge diode in [2]) or between the concentrations on the two sides of the channel (concentration diode in [2]).

2.3. Conductance model for tapered channel

The conductance measurements have been compared to the conductance model for straight channels given by Smeets et al. [23]. Here for the case with a negatively charge surface:

$$G = \frac{\pi r^2}{L}\left((\mu_+ + \mu_-)ne + \mu_+ \frac{2\sigma}{r}\right) \tag{13}$$

Where G is the conductance in Siemens (or A/V), r is the channel radius, L is the channel length, $\mu_{+/-}$ are the ions mobilities, n the concentration of a 1:1 electrolyte, σ the surface charge density and e the elementary charge. The term $(\mu_+ + \mu_-)ne$ corresponds to the bulk conductivity and the second term $\mu_+ \frac{2\sigma}{r}$ to the surface conductivity. The latter does not depend on the electrolyte concentration and consequently the channel conductance will saturate towards the surface conductance at low concentrations. At high concentrations, the second term becomes negligible compared to the first one and the channel conductance will follow the bulk regime. To estimate the conductance of a tapered channel, equation (13) has been modified by using a varying radius along x (see Figure 2), the distance along the channel from the base side:

$$r(x) = \frac{r_{base} - r_{tip}}{L} \cdot x + r_{tip}\ , with\ x\ from\ 0\ to\ L \tag{14}$$

$$dr = \left(\frac{r_{base} - r_{tip}}{L}\right) \cdot dx \tag{15}$$

$$dR_{bulk} = \frac{dx}{\pi r^2 ne(\mu_+ + \mu_-)} \tag{16}$$

$$R_{bulk} = \frac{L}{\pi ne(\mu_+ + \mu_-)(r_{base} - r_{tip})} \int_{r_{tip}}^{r_{base}} \frac{1}{r^2}\, dr \tag{17}$$

$$R_{bulk} = \frac{L}{\pi r^2 ne(\mu_+ + \mu_-)} \cdot \left(\frac{1}{r_{tip}} - \frac{1}{r_{base}}\right) \tag{18}$$

$$dR_{surf} = \frac{1}{\sigma \mu_+ 2\pi r} dx \tag{19}$$

$$R_{surf} = \frac{L}{\sigma \mu_+ 2\pi (r_{base} - r_{tip})} \int_{r_{tip}}^{r_{base}} \frac{1}{r}\, dr \tag{20}$$

$$R_{surf} = \frac{L}{\sigma \mu_+ 2\pi (r_{base} - r_{tip})} \cdot \ln \frac{r_{base}}{r_{tip}} \tag{21}$$

$$G_{taper} = \frac{1}{R_{bulk}} + \frac{1}{R_{surf}} \tag{22}$$

Where R_{bulk} is the bulk resistivity and R_{surf} is the surface resistivity. In this work, we assumed that K^+ and Cl^- ions have the same mobility within the solution with μ = 1.9 $\cdot 10^{-9}$ m^2/Vs [24][25].

3. Experimental Method

3.1. Membrane Fabrication

The samples used are the membranes *SM5200N* from *Norcada.* These are 2 (±0.5) µm thick silicon membranes supported on 300 µm thick silicon frames. The channels are milled through the membrane by using a focused ion beam (FIB) (*FEI Helios Nanolab 600*). The beam is driven by a coordinate list (streamfile), created with a *MATLAB* script containing the different parameters (coordinates, dwell time, number of passes). The current used is 0.46 nA and the acceleration voltage is set to 30 kV. To create the asymmetry, i.e. the tapered geometry, the FIB mills concentric disks with a linearly decreasing radius, with the largest disk having the base radius and the smallest the tip radius (see Figure 4 (a)). This operation is repeated on a number passes determined by dose tests on the frame supported side of the membrane until the membrane is punctured. The channels dimensions can be directly obtained with the scanning electron microscope imaging. Atomic force microscopy (AFM) imaging has been done the dose tests to characterize the profile of the tapered channel (see Figure 4 (b)).

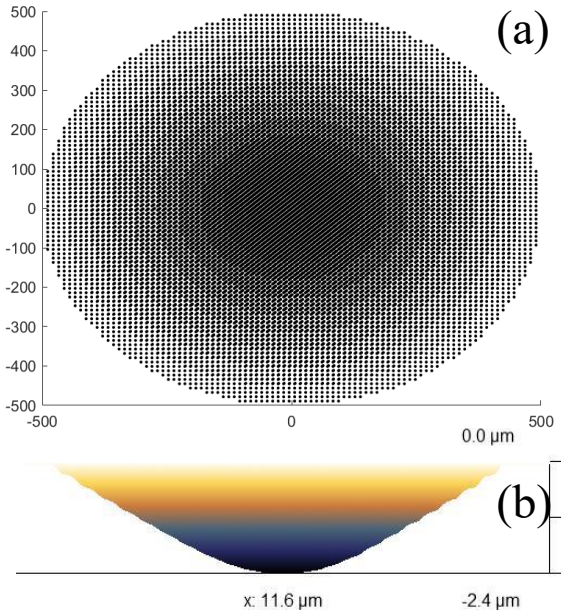

Figure 4: (a) Example of the pattern followed by the FIB to create the tapered geometry with ten concentric circles. The outer circle corresponds to the base radius and the inner one. corresponds to the tip radius. (b) Sideview of an AFM image of a dose test done on the frame supported side of the membrane.

3.2. Measurement Setup

During a previous attempt to measure the ICR, the membranes were glued on the bottom of a drilled laboratory beaker, which was then immersed in a larger second beaker. The two beakers being 2 reservoirs connected through the membrane's channel. However, the vertical configuration of the setup was often found to result in breaking of the membrane due to the pressure of the water column. Furthermore, gluing the membrane on the beaker does not allow

to remove it for further investigations such as Scanning Electron Microscope (SEM) imaging after the measurements. The development of a new non-destructive measurement setup was therefore necessary and done in this work. To avoid membrane breakage, the setup was designed to be in a horizontal configuration and allow easy membrane mounting. To facilitate sweeping the concentration, the reservoirs have to allow rapid solution exchange and avoid air trapping.

The design is shown at Figure 5 a). and is made of four main parts: two reservoirs and two PDMS gaskets. The reservoirs have been 3D printed in a transparent commercial polymer called *VeroClear*. The reservoirs have a tapered opening leading towards the membrane, to facilitate filling of the channel without trapping air. The PDMS gaskets have been casted in an aluminium mould, as shown in SUPPL FIGURE, and have an approximate thickness of 1 mm. The central pillar in the mould results in a channel, and an imprint of the membrane frame around the base of the pillar yielding an opening in the gasket to place the membrane. The membrane is placed in between the two gaskets and the whole setup is tightly squeezed and held together by using a laboratory clamp, see Figure 5 (b).

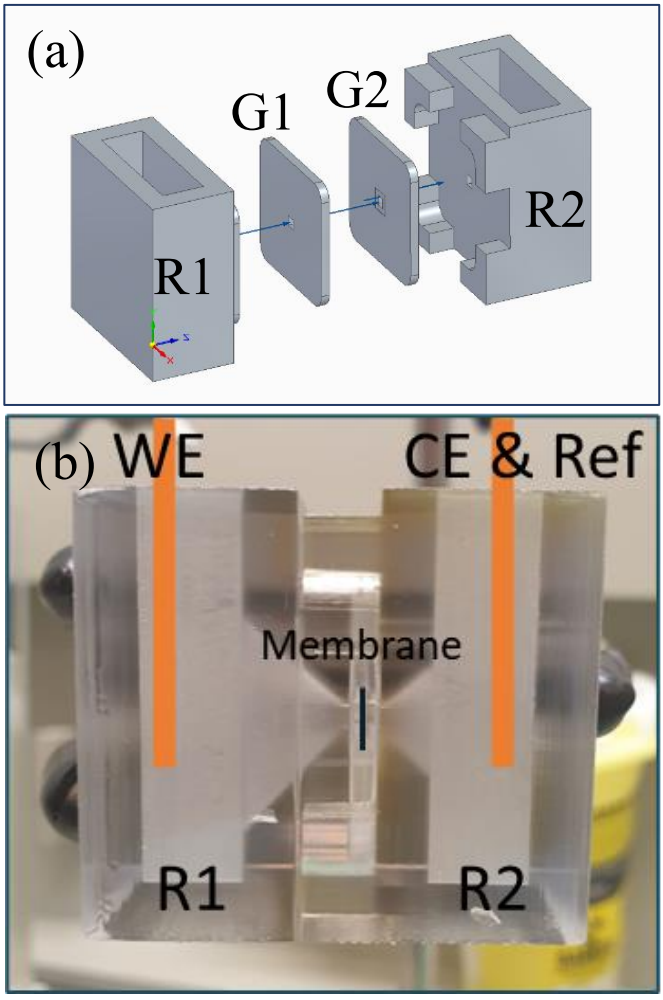

Figure 5: (a) 3D model of the setup showing the two reservoirs (R1 & R2) and the two gaskets (G1 & G2). (b) Picture of the mounted setup and schematic of the two wires Ag/AgCl electrodes. The black clamp holding the setup is visible on both sides.

3.3. Electrodes Fabrication

The protocol used to fabricate the Ag/AgCl wire electrodes is derived from the reference [26]. These electrodes have been chosen to have a minimal potential drop with the KCl solution. Therefore, the applied potential will fall only across the microchannel. The wires used are 99.99% pure Ag with a diameter of 0.35 mm. The wires are first immersed in 0.1M NHO_3 solution to remove the native oxide layer and other contaminants. They are rinsed with *MiliQ* water and connected to the working electrode of a potentiostat. A platinum wire, 99.99% pure with 0.2 mm diameter is connected to the reference and counter electrode. Both wires are immersed in a 3M KCl solution and a 2 V potential is applied to the working electrode for 10 minutes.

The Ag/AgCl wires electrodes are then stored in the 3M solution and can be reset by following the same protocol. Their stability over time has been controlled by measuring the evolution of the open circuit potential (OCP) between the wire electrodes and a leakless reference electrode during 12 hours.

3.4. Gold Coating

The gold coating of the membrane has been done by sputtering (*Leica EM ACE600*). To improve the Au coating adhesion, a 4.8 nm thick Cr layer is deposited before the 50 nm Au layer.

3.5. Conductance measurements

The conductance measurements are done through the membrane by using 2 Ag/AgCl wire electrodes described in section 3.3 in a 2-electrode setup. The membrane separates the two reservoirs of equal concentration. The reservoirs are slowly filled alternatively to equal liquid heights to avoid pressure differential between the two sides. Importantly for the sign convention in the next chapter, the working electrodes are placed on the largest opening side of the channel and the counter electrode (which is connected with the reference electrode) is placed on the other side.

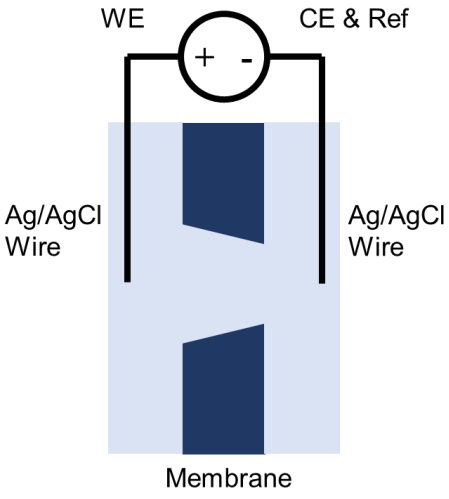

Figure 6: Schematic description of the setup for the conductance measurements.

The staircase voltammetry technique (SCV), schematically shown in the Figure 7, is used to measure the current response to the potential sweep. With this technique the potential is cycled from an initial potential (-1 V), to a final potential (1 V), by incrementing the potential in 0.05 V steps. Each potential is kept for a period of 10 s, where the measured current is the average of the final 0.5 s of each step.

This technique allows to avoid noises that could appear during classical cyclic voltammetry measurements by averaging the current over the sample width and to reduce the overall measurement time.

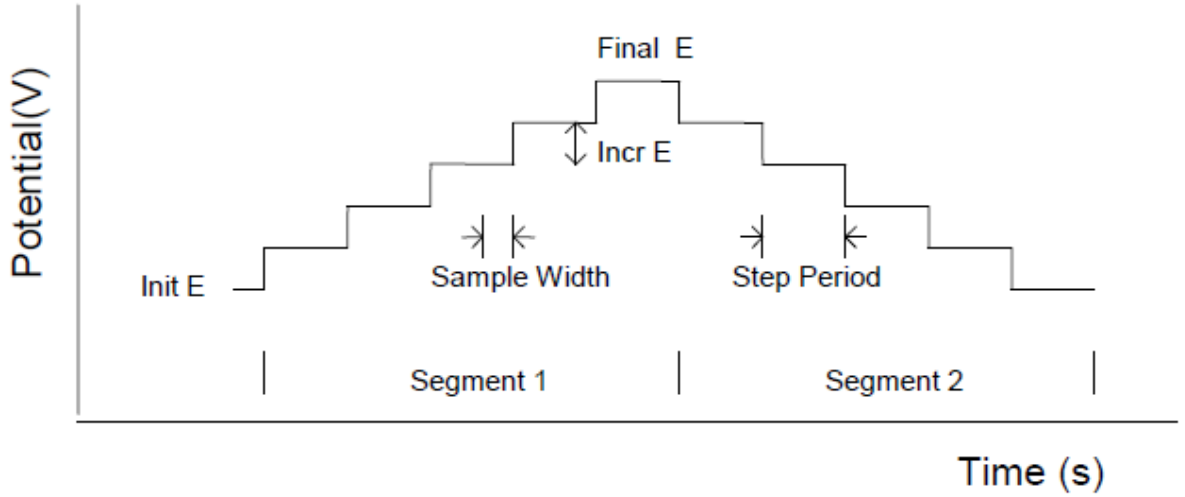

Figure 7: Staircase voltammetry technique of the CH Instruments potentiostat. Taken from the user manual of the software "Chi760".

4. Results and Discussion

4.1. Effect of concentration dependent surface charge on ICR

This section aims to present the effect of the surface charge on the current rectification. As shown in section 2.2, the Dukhin number takes into account the surface charge density and reflects the relative contribution of the surface conductivity to the total conductivity. Therefore, for a fixed geometry, the surface charge determines the concentration range at which the rectification can occur. Or alternatively, for a known surface charge, one can determine the pore geometry needed to possibly achieve rectification at a desired concentration range.

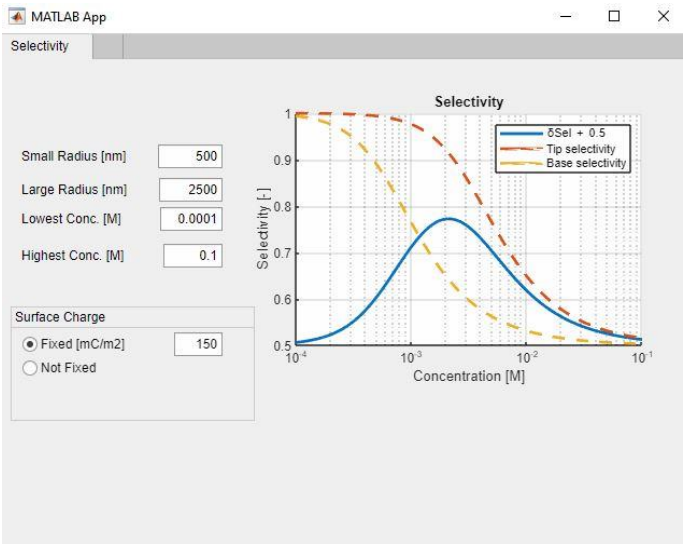

Figure 8: MATLAB app developed to explore the behaviour of the selectivity model for different parameters such as the channel's geometry and the surface charge density. δSel is the selectivity difference shifted by +0.5 for clarity.

To rapidly visualise the effect of surface charge variation on the selectivity within the channel, a user-friendly MATLAB applet has been created in this thesis. The app allows to quickly change the parameters of the selectivity model, i.e. the base and tip radii and the surface charge of the channel.

Figure 9 illustrates the selectivity model for an increasing surface charge density for a fixed channel's geometry with 1500 nm a base radius and a 500 nm tip radius. It clearly appears that an increase in the surface charge leads to a shift of the ICR peak towards higher concentration; almost two orders of magnitude in concentration between 5 mC/m^2 and 50 mC/m^2.

Up to this point, the charge density of the SiO_2 surface was assumed to be constant independently of the electrolyte concentration. However, it is not necessarily the case as shown by Taghipoor et al. [27] and Smeets et al. [23]. The surface charge density of SiO_2 in KCl solution is shown to be pH dependent as well as dependent on the concentration of KCl itself.

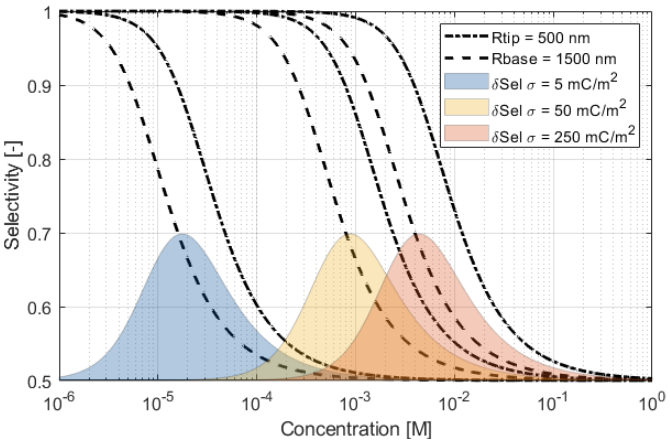

Figure 9: Selectivity model for a channel with a base radius of 1500 nm and a tip radius of 500 nm with a charge density of 5, 50, and 250 mC/m^2. δSel is the selectivity difference and shifted by +0.5 for figure clarity.

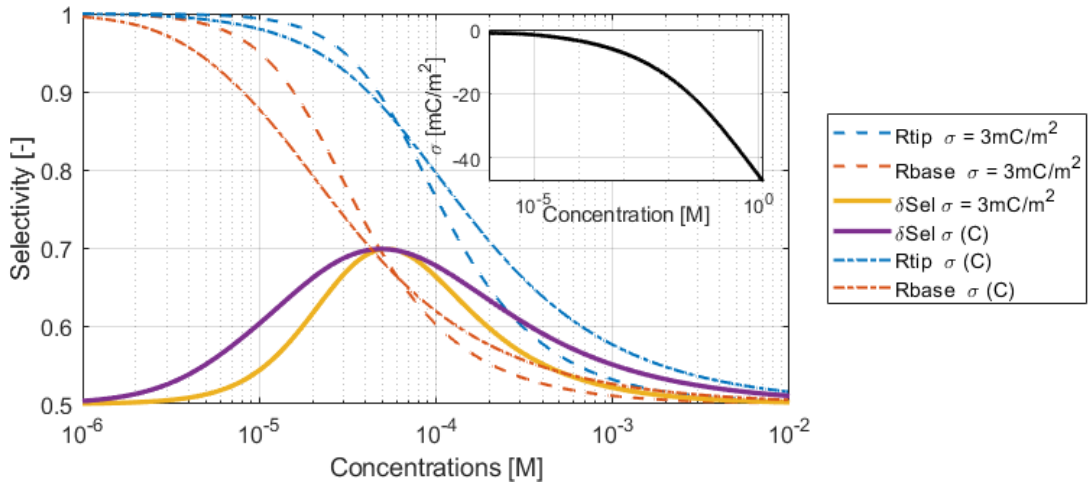

Figure 10: Selectivity difference (δSel) for a 3 mC/m² constant surface charge density (yellow) and a concentration dependant surface charge density (purple). The dependency has been taken from Taghipoor et al. for pH = 6 and is shown in the inset. The tip and base radii are respectively 500 nm and 1500 nm. The selectivity difference δSel has been shift by +0.5 for figure clarity.

This concentration dependency of the surface charge density is depicted in Figure 10. The concentration dependency of the surface charge is interpolated from reference [27] for a pH = 6 (which is the expected pH of our solutions in ambient conditions), which ranges from 3 mC/m^2 at 10^{-4} M to 30 mC/m^2 at 0.1 M. This dependency leads to broader ICR range for the same channel geometry as shown by the purple line.

4.2. Leakage current

To identify the magnitude of noise in our measurements, SCV measurements have been conducted on a fresh membrane without any channel at four different solution concentrations (10^{-4}, 10^{-3}, 10^{-2} and 10^{-1} M). The average IV curve of these measurements is presented in Figure 11 and the measured IV curves are given in appendix (Figure 23). The figure shows that there is a background current which we understand to be the leakage current through the membrane. We observe that the leakage current is non-linear, and of negligible magnitude at low potentials (~< |0.5| V). It should be noted that while the leakage current appears to be independent of the reservoir concentration, the measured ionic current through the channel does

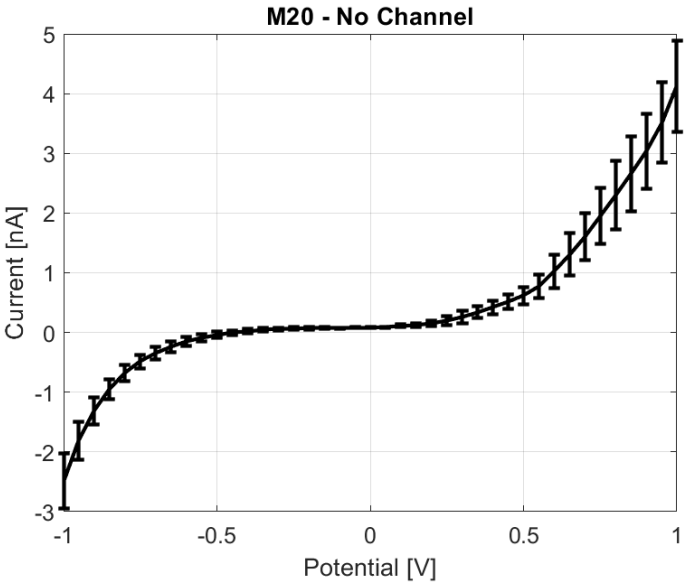

Figure 11: Average IV curve for the membrane M20 without any channel. The measurements were done at four concentrations: 10^{-4}, 10^{-3}, 10^{-2} and 10^{-1} M.

depend on the bulk concentration, so that the signal to noise ratio becomes worse as the concentration decreases.

The presence of such leakage currents has been confirmed by the membranes' supplier and the current levels correspond to ones in the literature [28].

To ensure sufficient ionic current to be measured with the background leakage current, the channels have been designed to have an expected ICR peak at high concentrations, i.e. in the 10^{-2} M range. However, as will be shown in the next section, the measurements done in the 10^{-4} M range for the membrane with a channel, still show a non-linear behaviour.

For further investigations, one should consider passivating the membranes' surface by depositing a dielectric layer. Lee et al. [28] showed that leakage current in Si-based nanoporous structures could be reduced from tens of nA to tens of pA by depositing a 30nm thick layer of either Al_2O_3 or SiO_2.

4.3. Conductance of single micro channels

Table 1 presents the geometrical parameters of the membranes used for the conductance measurements as measured by the SEM right after the fabrication. The membranes M17 and M22 are the tapered microchannels and the membranes M19 and M24 are the so-called reference channels, or straight channels where the dimensions are made to be the same as the large/small opening of the tapered channels, respectively. The membrane M20 has been used to measure the leakage current shown in section 4.2 . On the membrane M23, an array of 5 x 5 channels has been milled. This array membrane is further described in the section 4.5. Figure 12 shows two SEM images of the single channels M22 and M24. Supplementary images of other membranes are provided in appendix (Figure 26 to Figure 30). The membrane M18 has been coated with a gold layer for a surface charge modulation attempt (see section 4.6).

*Table 1: Membranes' geometries. * Parameters of the central channel of the 5x5 channels array.*

Membrane	Tip radius [nm]	Base Radius [nm]	Base/Tip Ratio [-]	Thickness [nm]
M17 Tapered	520	1450	2.79	2000±500 nm
M18 Tap. Gold	430	1475	3.43	2000±500 nm
M19 Ref.	590	590	1	2000±500 nm
M20 w/o chan.	-	-	-	2000±500 nm
M22 Tapered	410	1480	3.61	2000±500 nm
M23 Array	335*	1420*	4.24	2000±500 nm
M24 Ref.	1500	1500	1	2000±500 nm

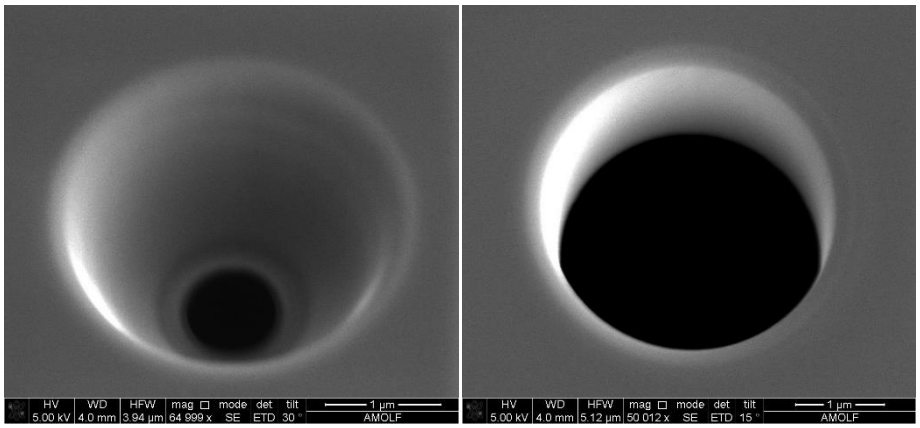

Figure 12: SEM images of the tapered channel M22 (left) and the reference channel M24 (right) done right after the fabrication.

The conductance measurements were done as described in section 3.5 for concentrations between 10^{-4} and 10^{-1} M. This specific range has been chosen for several reasons. First, from a practical point of view, solutions with concentrations higher than 0.1 mM, are easier to obtain, to control and show a higher current magnitude. The current-voltage behaviour is expected to be influenced by the leakage current for the lowest concentrations, where channel conductance is too small. Second, this is the range were ICR has been observed during the previous measurements within the group on similar channel geometries. The channels were specifically chosen to be larger than the EDL (see Figure 1), especially for the tip radius, and to remain easily fabricable with the FIB.

The current-potential curves (IV) for the four singles channels are shown in Figure 13. As the magnitude of the current spans several orders of magnitude over the concentration range, the IV curves are normalized for clarity. The leakage current at V = 0, 0.07 nA is taken as an offset of the measurement and has been subtracted from the measured IVs. The IVs are then normalized by the current value at -0.5 V. This latter potential has been chosen in regard of the non-linear behaviour due to the greater effect of the leakage current at potential above (below) 0.5 V (-0.5V), as shown in section 4.2, which is especially relevant for the lowest concentrations where the measured current is in the nA range.

For the straight channels M19 and M24, the current response is expected to be linear with the potential. Up to $1{\cdot}10^{-3}$ M, it is however not the case, with the IVs presenting a S-shape. This has been understood to be the effect of the contribution of the leakage current on the measured one. Indeed, at the lowest concentrations, the current measured is close to the leakage current depicted in Figure 11. The non-normalized IV curves are given in appendix. For the membrane M19 above $1{\cdot}10^{-3}$ M, where the current magnitude is significantly larger than the leakage current, the curves show a linear behaviour as expected for the bulk conductance of a straight channel. M24 does not show the same strong linearity with a slight deviation of the current in the positive potential range. This deviation appears for the concentrations between $6{\cdot}10^{-4}$ M and $4{\cdot}10^{-3}$ M where the normalized current reaches values between 1 and 1.5. Therefore, this can be seen as a current rectification ($|I(+V)| > |I(-V)|$) in the inverse direction of the rectification expected in our configuration for the tapered channels ($|I(+V)| < |I(-V)|$). This behaviour is not expected, especially when compared to M19. From the larger dimension of M24, the bulk

conductance should be dominant at lower concentrations compared to a smaller channel. This non-linearity cannot be immediately explained but could go towards a possible clogging, previously mentioned in section 4.3, that would have changed the effective geometry in the channel.

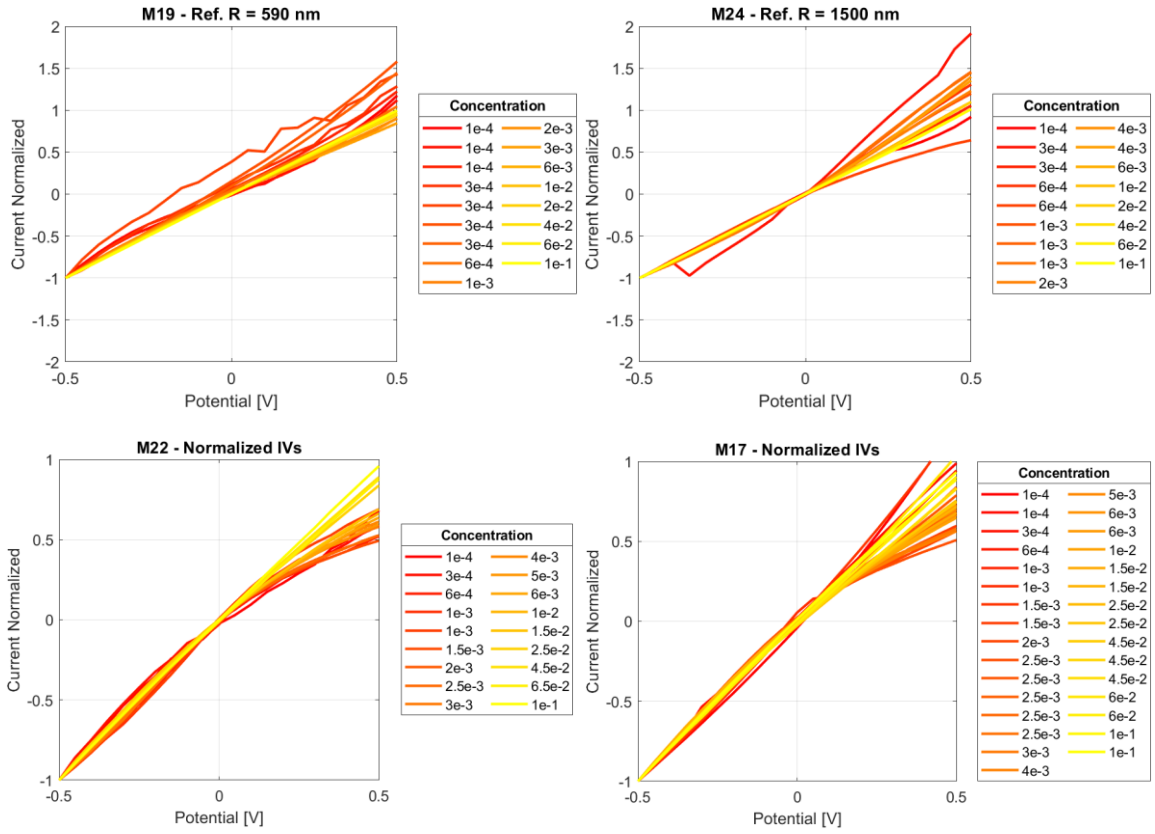

Figure 13: Normalized current-potential curves for the two references straight membranes (M19 and M22) and the two tapered membranes (M17 and M22). The leakage current at 0V, 0.07nA, has been subtracted to the IVs and it has been normalized by I(-0.5V).

The current rectification is clearly visible in the normalized IV of both tapered channels. It can be seen qualitatively on the positive potential side where the curve starts linear at the lowest concentrations (in red) and then bends down, indicating a lower conductance state. The curve first bends with the increasing concentration and reaches a maximum (in orange). With the concentration keeping increasing, the curve bends up again towards a linear response (in yellow). These results clearly match with the behaviour predicted by the selectivity model (see section 2.2) and confirm that the ionic current rectification is possible at the micro scale as predicted in the references [2], [6].

Figure 14 presents the differential conductance at 0 V derived from the current-potential curves for the two reference membranes M19 and M24. The measurements are compared to the conductance expected for these geometries, calculated by equation (13) and shown by the two continuous blue and green areas. The surface charge has been set to zero, therefore the channel conductance is only determined by the bulk solution contribution. The areas' boundaries are defined by uncertainty for the membranes thickness, i.e. 2 ± 0.5 µm.

Within this concentration range, for both channels, the conductance shows a linear behaviour on the logarithmic scale with a slope matching the model. The latter is determined by the bulk conductance of the solution. Therefore, the conductance appears to be mainly determined by its bulk contribution for these straight channels.

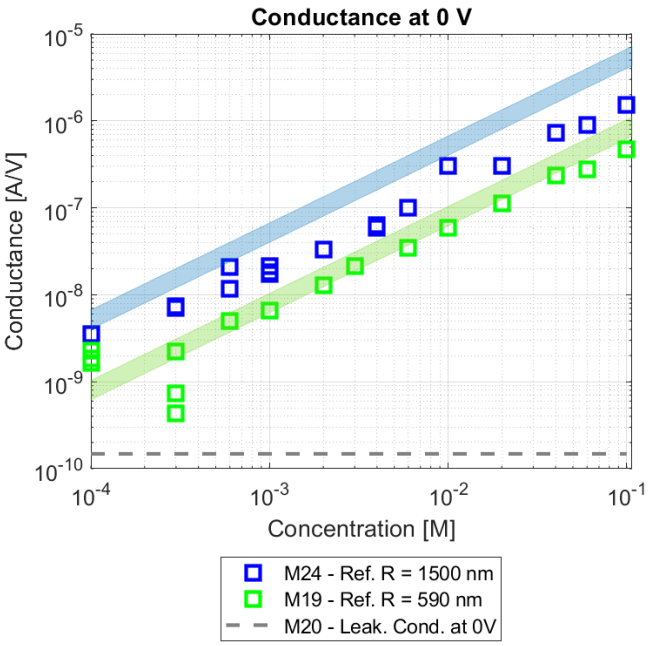

Figure 14: Conductance of the two reference channels around 0 V. The two shaded areas are the respective bulk conductance for a membrane thickness between 1.5um and 2.5um with a zero-surface charge.

Concerning the magnitude of the conductance, which is defined by the geometry of channels, the small reference channel M19 seems to match with the theory. However, the larger one, M24, shows a lower conductance than its prediction. A variation in its geometry could explain this difference. A thicker membrane leads to a lower conductance as shown in the equation (13). Considering the same radius of 1500 nm, a thickness of 5 µm would bring the predicted conductance towards the measured one. This hypothetical thickness is twice larger than the upper tolerance limit given by the supplier and therefore seems unlikely. However, the thickness has not been measured. The second possibility is a variation in the radius of the channel. By keeping the thickness range between 1.5 and 2.5 µm, a radius of 900 nm, i.e. a reduction of 74% of the channel's section, would bring down the theoretical conductance towards the experimental data. Such a reduction could be explained by an unfortunate clogging of the channel. Although unlikely, this clogging is not impossible and has been observed on other channels as shown in section 4.7.

Figure 15 presents the conductance for the two tapered membranes M17 and M22. Three conductances extracted from the current-potential curves are shown: The differential conductance around 0 V and the average differential conductance between (-) 0.25 V and (-) 0.5 V. The measured conductance is compared to the theoretical one for a tapered channel, as well as for straight channels corresponding to the respective base and tip radii at a surface charge density $\sigma = 30$ mC/m^2. The latter has been given from a visual fit where the theoretical model saturates at low concentrations to the surface conductance.

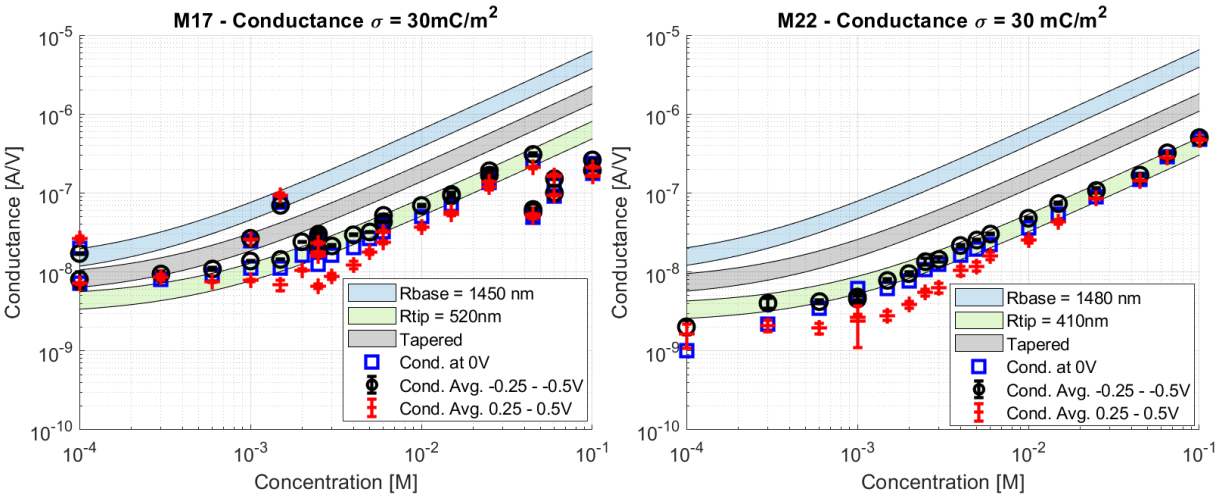

Figure 15: Membrane M17 and M22. Conductance extracted from the IV curves measured. The shaded areas depicted the conductance model for σ = 30 mC/m² for the corresponding radii of M22 and M17 and a membrane thickness between 1.5 and 2.5 µm. The red and black markers are the average conductance for respectively V>0 and V<0. The blue markers are the conductance around 0V.

At the highest concentrations, above 10^{-3} M, the two membranes follow the expected bulk regime, expressed by a linear slope in the log scale. However, both of them do not have the expected conductance for a tapered channel (grey shaded area) but rather match with the conductance model for a straight channel with the radius equal to that of the tip (green shaded area). For both membranes, it appears that the conductance at low concentrations, approx. $< 10^{-3}$ M, is mainly determined by the surface conductance as expected by the model. This can be seen by the slope variation towards a saturation. The membrane M22 seems to follow the surface conductance of the tip radius straight channel for a surface charge density in the order of 30 mC/m^2. The second membrane M17 saturates at a higher conductance in the surface regime and therefore could indicate a higher surface charge density present within the membranes. Overall, the conductance of the tapered channels appears to be limited by the smallest geometry, i.e. the tip opening, against the expect conductance of a tapered channel lying in between the respective conductance of the tip and base radii straight channels.

For both membranes, the conductance at negative bias (in red) is similar to that found at 0V for concentrations below 0.6 mM and above 25 $\cdot 10^{-3}$ M, while at positive bias the conductance deviates from that at 0V and negative bias for concentration below 0.25 $\cdot 10^{-3}$ M. The deviation between the conductance for the negative bias and the positive bias is more pronounced between $1 \cdot 10^{-3}$ M and $4 \cdot 10^{-3}$ M where the transition from surface to bulk conductance occurs. It is the first indication of different conductivities at positive and negative bias, i.e. ICR

4.4. Ionic Current Rectification in single asymmetric channels

The ICR is quantitatively depicted in Figure 16 where each tapered channel is compared to the two reference channels (left y-axes) and the selectivity model (right y-axes). As previously mentioned, the two straight channels M17 and M24 are expected to present only a pure ohmic behaviour and therefore are expected to show an ICR = 1, independently of the electrolyte concentration. Above $6 \cdot 10^{-4}$ M, the membrane M19, depicted in green, show ICR values slightly above 1 with a maximum around 1.2 at $3 \cdot 10^{-3}$ M. At the lowest concentrations, the ICR values below 1 are explained by the non-linear behaviour due to the leakage current influence. The second straight membrane M22 shows ICR values below 1, which indeed illustrates the slightly rectifying behaviour forementioned. However, for both straight channels, these ICR ratio are definitely much closer to unity than the tapered channels' ratios. Therefore, the references channels can be considered as non-rectifying compared to the tapered channels.

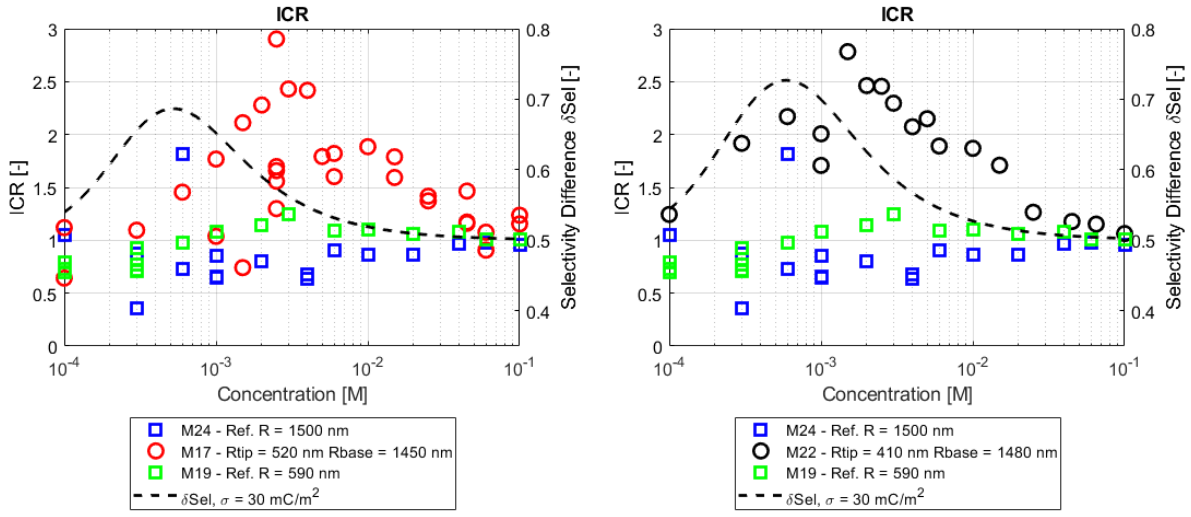

Figure 16: Ionic Current Rectification for M17 (left) and M22 (right) versus concentration. The ICR measured for the references channels is depicted in blue and green. The selectivity difference (δSel) from the model, is depicted by the black dash line for the corresponding geometries of M17 and M22 with σ = 30 mC/m² on the right y axis.

The first tapered channel M17 (Figure 16, left) shows ICR values following the bell shape trend expected from the selectivity model, despite a few outlying points. The ICR is close to one at the lowest concentration and rises with increasing concentration. It reaches its maximum value, ICR = 2.9, at $2.5 \cdot 10^{-3}$ M and decreases again with the concentration to ICR = 1.2 at $1 \cdot 10^{-1}$ M. The experimental values are compared to the selectivity model, from reference [6] and introduced in section 2.2, where it is important to note that selectivity model gives the difference in selectivity between the tip and base ((δSel), and therefore can only be compared qualitatively to the measured ICR, for M17's geometry and a surface charge density σ = 30 mC/m². This value has been extracted from the conductance versus concentrations plot as explained in the previous section. The concentration at which the ICR reaches its maximum is higher than the expected one from the selectivity model, $1.5 \cdot 10^{-3}$ M and ~$0.5 \cdot 10^{-3}$ M respectively. It suggests a higher surface charge density than 30 mC/m² inside the pore. Considering the same channel geometry, a surface charge density of 150 mC/m² would be necessary for the model to match the maximum ICR concentration. This value does not match the conductance at which the channel saturates at the lowest concentrations (see Figure 15). Furthermore, the selectivity

model has been calculated for a constant surface charge density, which is not necessary the case as was shown in section 4.1.

The second tapered channel M22 also shows ICR ratio values following a bell shape trend. At the lowest concentration 10^{-4} M, the ratio is ~ 1and already rises to 2 at the next concentration $3 \cdot 10^{-4}$ M, against around 10^{-3} M for M17 to reach the same value. The ICR ratio keeps rising with the concentration up to $1.5 \cdot 10^{-4}$ M, where it reaches its maximum of 2.8. The ratio then decreases with the concentration and reaches 1 again at the highest concentration at 10^{-4} M. The membrane is also compared to the selectivity model for the corresponding channel geometry with a surface charge density of 30 mC/m^2. Here again the concentrations at which the selectivity model and the measured ICR ratio reach their respective maximum do not match, with respectively $\sim 0.6 \cdot 10^{-3}$ M and $1.5 \cdot 10^{-3}$ mM. A theoretical surface charge density of 100 mC/m^2 in the selectivity would be necessary to match with the measured ICR bell. Again, this value does not match the conductance behaviour of the channel M22 (see Figure 15).

Considering such differences, it should be noted that the surface conductance dominates over that of the bulk at low concentrations in the conductance model. As explained the section 4.1, the surface charge density is expected to increase with the concentration and where the surface charge density extracted from the conductance model can only be determined at the low concentrations where the saturation occurs ($<1 \cdot 10^{-3}$ M). Even with an increasing surface charge density at higher concentrations, the values that the selectivity model would require to match its maximum's concentration with the ICR bells seem unlikely. However, the surface charge density within the pore has not been measured at all concentrations and effects of the focused ion beam on the Si surface charge, through e.g. roughening or the use of Ga atoms, are unknown. Furthermore, the selectivity model has been developed on the assumption of a slowly varying geometry, i.e. a high aspect ratio between the membrane's thickness and the channel diameter. In our case, this assumption could not be fulfilled as the thickness dimension is close to that of the channel openings.

4.5. Conductance in asymmetric micro-channels array

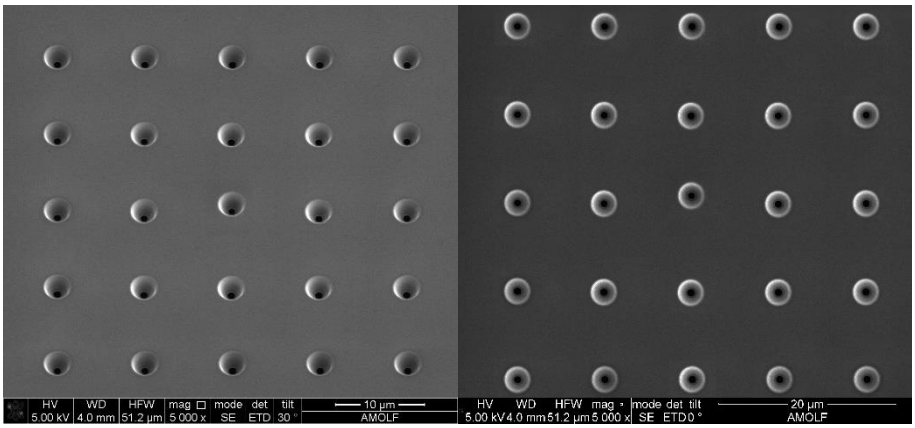

Figure 17: Membrane 23. 5 by 5 tapered channels array with a pitch of 10µm. The base radius is approximatively 1420 nm and the tip radius 335 nm. The array has been made on two separated runs. First the central channel and secondly the 24 other channels.

Figure 17 shows SEM images of a 5 by 5 array of tapered channels. The channel situated on the centre has been first fabricated with the FIB; its dimensions are shown in Table 1. The 24 other channels have then been fabricated in a second run, which explains the small misalignment of the centre channel with the rest. All channels have been made with the exact same FIB parameters and the pitch, centre from centre, is 10 µm.

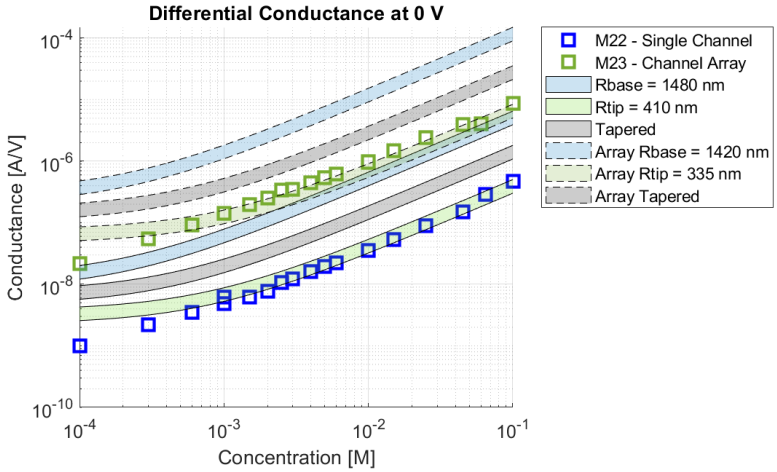

Figure 18: Differential conductance at 0V for the single tapered channel M22 and the channel array M23. The shaded areas depicted the conductance model for σ = 30 mC/m² for the corresponding radii of M22 and M23 (central channel) and a membrane thickness between 1.5 and 2.5 µm. For the array, the model is used to calculate theoretical conductance of a single channel. This conductance has then been multiplied by the number of channels, 25.

Using the model of parallel conductance, the total conductance of the array is therefore expected to be the sum of the 25 individual channels. It naturally brings up the question of what would be the effect of an array configuration on the ionic current rectification. Figure 18 presents the measured conductance at 0 V for the array M23 (green). The conductance of the single tapered channel in membrane M22, which has dimensions close to the channels in the array, is also present for comparison. By comparing the two at 10^{-4} M, it appears that the conductance of the array is approximatively 20 times higher than the one of the single, which is close to the expected conductance from the parallel conductance model.

Figure 19 below shows on the left the normalized current-potential curves for the array M23. It clearly shows that the current response is linear for almost all concentrations and there is no bending due to a lower conductance state in the positive potential range as seen for the single tapered channels. On the right of the figure, the ICR ratios measured for the array is compared to the ICR ratios of the single tapered channel M22. Here again, it clearly appears that no rectification occurs for the array membrane and that all values are close to 1, as seen for the reference straight channels.

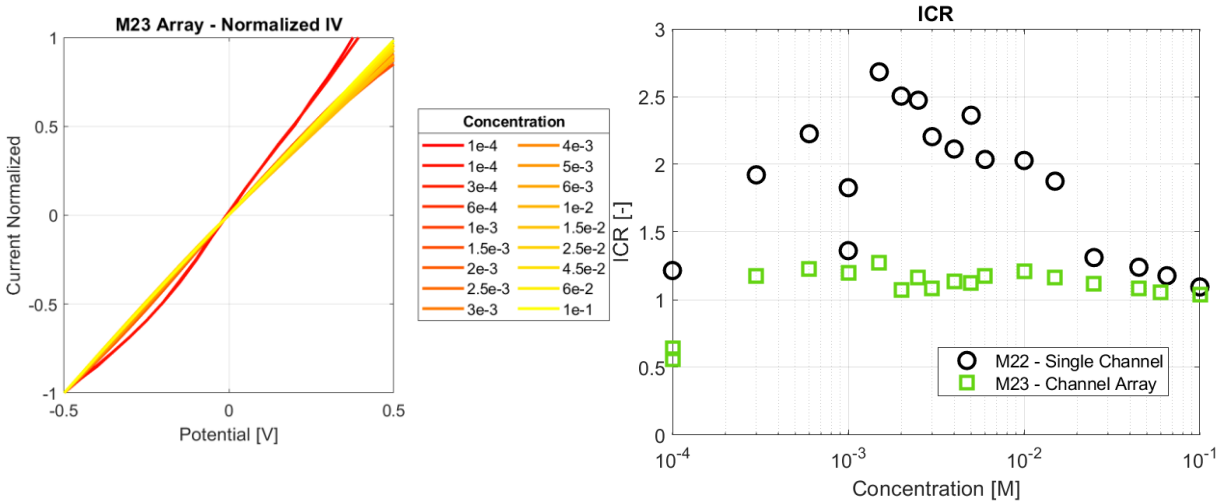

Figure 19: Left: Normalized current-potential curves for M23. Right: ICR ratio measured on the array compared to the single tapered channel M22.

From these results, we can state that an array of tapered channels cannot be seen at the sum of 25 single channels, from the rectification point of view and at least for this pitch of 10 µm. This result suggests channel to channel interaction and is not without importance. These interactions could limit the achievable rectifying current density of membranes using such micro tapered channels. Indeed, in osmotic power generation for example, to have a sufficient power generation, the pore density within the membrane should be as high as possible. However, it has also been shown that a too high pore density could lead to efficiency reduction [29].

4.6. Surface Charge Modulation

As seen at section 4.1, the surface charge density within the channels controls the concentration at which the maximum rectification occurs for a given channel geometry. Therefore, the ability of modulate dynamically the surface charge could allow a dynamic control over the rectification and the ionic current through the channel. Such abilities have particular interests in ionic devices such ion pumps or ionic transistors [18].

In order to attempt such modulation of the surface charge, a tapered channel has been coated with a 5 nm Cr layer as adhesion layer and a 50 nm Au layer. Applying a potential on the gold layer would lead to a variation of the surface charge density and consequently alter the rectifying behaviour of the channel.

The first measurements have been done on the channel M18 (Table 1) without applying any potential on the gold layer. The current response appears to be strongly instable and show a strong non-linear behaviour. This behaviour is similar to what has been observed for the leakage current through the fresh membrane explained in section 4.2, suggesting a background current limiting the current response of the channel. Furthermore, Cl^- ions are known to show chemisorption on the gold surface [30]. Further investigations could unfortunately not be conducted within the frame of this work. However, similarly to the non-coated membranes, the surface passivation with an oxide layer coating could reduce the leakage current through the membrane as suggested in the references [18], [28], [30].

4.7. Experimental Limitations

From the experimental point view, several obstacles appeared during the project. During the early conductance measurements, the formation and/or the trapping of air bubbles in front of the channel's openings led to current cutting. The probable reason of this is the air trapped between the two PDMS gaskets during the mounting that could consequently slowly leak at the interface with the sample. This has been overcome by depositing solution droplets on both side of the membranes before the mounting within the setup and by more tightly closing the clamp holding it. However, even in absence of visible bubbles in front the channel, the current could be cut from time to time. It has been recently shown that micro air bubble could be trapped in the pore, especially with hydrophobic surfaces, and therefore limit the ionic flux. These trapped bubbles could be flushed out of the channel by applying pressure or (less effectively) a potential [31].

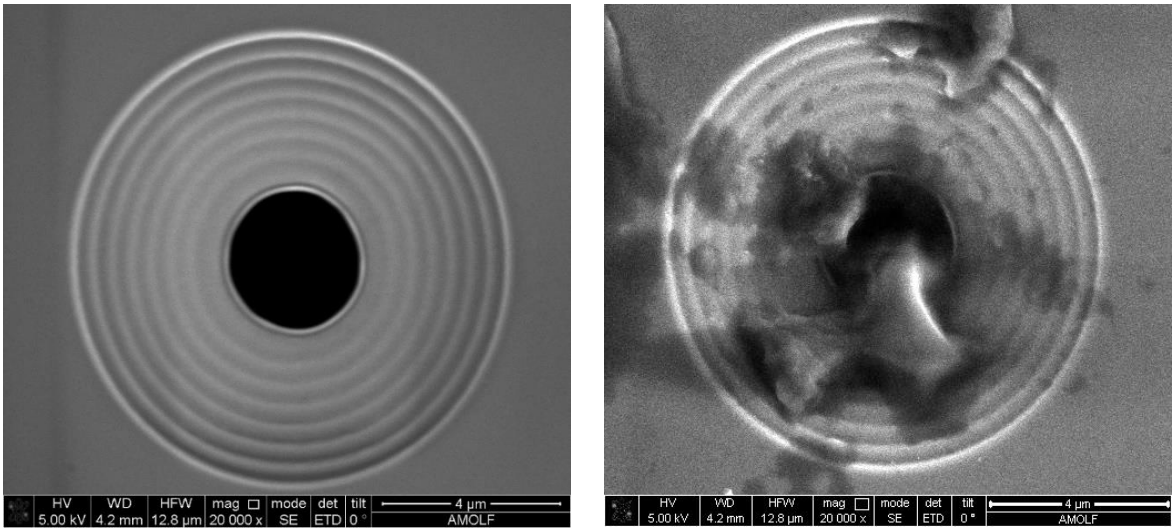

Figure 20: SEM images in top view of a tapered channel. Left: After the FIB milling. Right: After the conductance measurements. Note that this channel has dimensions larger than the channels presented in Table 1. Rtip = 1420 nm , Rbase = 5000 nm. Membrane Thickness = 2000nm

During SEM imaging performed on the membranes after the conductance measurements, it appears that contaminations could clog the channels as shown in Figure 20. The nature of this contamination is unknown. However few cleaning attempts have been made. The contamination did not dissolve in water soaking and could not be removed by plasma cleaning. Furthermore, the contamination could not be verified under EDX. This kind of clogging could alter the effective geometry of the channel and is therefore expected to change the current response away from the rectification phenomenon.

5. Conclusion

Blue energy remains an untapped and large source of energy and the existing technologies to capture it suffer from the low efficiency of the nanoporous membrane used in the processes. This low efficiency is attributed to the high resistivity of the nanopores to the ionic current. New membranes using micropores presenting an ionic current rectification behaviour could therefore reduce this resistivity and consequently increases the conversion efficiency of such membranes.

With this long-term objective in mind, this project aimed to investigate the possibility of ion rectification current at micrometric scale in asymmetric silicon channels. Following recent theoretical demonstrations of ICR at such scale without any chemical modification of the channel, recent results within the group have experimentally shown it for the first time. The first objective of this work has been to confirm and reproduce these results. A new measurement setup has been developed to facilitate the reproducibility of the experiments and to reduce the risk of membrane breaking during the measurements. This setup allowed us to reproduce successfully the previous results and to confirm them. Furthermore, the use of this setup indeed significantly improved the lifetime of the membranes and made the measurement much easier. In this work, the two tapered membranes presented have shown a rectification ratio following the concentration dependent behaviour trend predicted by the selectivity model, where maximum ratios of 2.9 for M17 and 2.8 for M22 were reached.

From these results, few limitations have been identified. The influence of the leakage current of the membrane over the channel response has limited the measurements at the lowest concentration by deviating the current response from the linear behaviour expected. This limitation could be overcome by the passivation of the membrane with an oxide coating such as SiO_2. Another obstacle has been the limited knowledge on the surface charge density present in the channels and therefore further investigations should be done to measure this surface charge density, to know its evolution with the electrolyte solution or its potential modification during the ion bombardment during the fabrication. Furthermore, the tapered channels conductance followed the conductance model predicted for a straight channel with a radius corresponding to the tip opening of the tapered geometry. This suggests than the channels currently used do not fulfil completely the assumption of a slowly varying geometry on which the theoretical model are based. There is therefore an interest to explore different membranes thicknesses.

An attempt to show ICR on a 25 channels array has been made. Despite showing the correct magnitude compare to single channel membrane, the current did not show a rectifying response. This result suggests channel to channel interactions that could limit the current density of such multi channels membranes and therefore limit the conversion efficiency of such membranes.

The second of objective of the work was to attempt dynamic modulation of the ICR by tuning the surface charge density within the pore with an external potential applied on a gold coating. The current has shown very unstable responses suggesting the presence of a background current and the modulation has not been achieved. Further investigation should explore the possibility of oxide coating on the gold layer to avoid side reactions at the surface.

In conclusion, we have successfully shown the ICR phenomena in micrometre scale tapered Si channels, as predicted by the recent theoretical researches, in a newly developed and more controlled setup, in a more reproductible manner than for the previous results. Finally, this work allowed us to more clearly identify several limitations on the ICR phenomena and to define few directions for further investigations, really paving the way to a dynamic control and modulation of the ICR in asymmetric Si-channels.

6. Acknowledgments

Spending these 25 weeks at AMOLF for this project has been a great pleasure and an inspiring experience. Despite the pandemic situation, I was fortunate enough to find a working environment full of lab work and full of inspiring (online) talks, (online) colloquiums and other science sharing among the colleagues.

This experience and work could not have been possible without my supervisors. Firstly, I would like to thank Prof. Fontcuberta at EPFL to given me the opportunity to conduct my master thesis abroad and to introduce me to Dr. Alarcón Lladó.

I would also like to warmly thank Esther for accepting me as a master student in her group for my master thesis. Your advices, questions and the discussions we had all along the project have been a great source of motivation and knowledge to me. You really built an inspiring group and environment around you, which ultimately leads to great science.

I would like also to acknowledge and thank my direct supervisor, Mark. Your time, patience and availability (even while finishing writing your thesis!) to answer my questions, help me to start in the lab and for the numerous feedbacks, have been a tremendous help. Thank you also to have supported the continuous live flow of images during my experiments in the lab.

Thanks also to all other members of the groups for the all the nice talks, advices and the fun in the lab. I'm pretty sure we will see each other again (in person!). Finally, I would like to thank all the other members of AMOLF for the help in the clean rooms and in the lab.

7. References

[1] L. Bocquet and E. Charlaix, "Nanofluidics, from bulk to interfaces," *Chem. Soc. Rev.*, vol. 39, no. 3, pp. 1073–1095, 2010.

[2] A. R. Poggioli, A. Siria, and L. Bocquet, "Beyond the Tradeoff: Dynamic Selectivity in Ionic Transport and Current Rectification," *J. Phys. Chem. B*, vol. 123, no. 5, pp. 1171–1185, 2019.

[3] L. Jubin, A. Poggioli, A. Siria, and L. Bocquet, "Dramatic pressure-sensitive ion conduction in conical nanopores," *Proc. Natl. Acad. Sci. U. S. A.*, vol. 115, no. 16, pp. 4063–4068, 2018.

[4] E. C. Yusko, R. An, and M. Mayer, "Electroosmotic flow can generate ion current rectification in nano- and micropores," *ACS Nano*, vol. 4, no. 1, pp. 477–487, Jan. 2010.

[5] M. Nishizawa, V. P. Menon, and C. R. Martin, "Metal Nanotubule Membranes with Electrochemically Switchable Ion-Transport Selectivity," no. May, 1995.

[6] S. Dal Cengio and I. Pagonabarraga, "Confinement-controlled rectification in a geometric nanofluidic diode," *J. Chem. Phys.*, vol. 151, no. 4, Jul. 2019.

[7] V. V. R. Nandigana, K. Jo, A. Timperman, and N. R. Aluru, "Asymmetric-Fluidic-Reservoirs Induced High Rectification Nanofluidic Diode," *Sci. Rep.*, vol. 8, no. 1, Dec. 2018.

[8] E. B. Kalman, I. Vlassiouk, and Z. S. Siwy, "Nanofluidic bipolar transistors," *Adv. Mater.*, vol. 20, no. 2, pp. 293–297, 2008.

[9] Y. Zhang and G. C. Schatz, "Conical Nanopores for Efficient Ion Pumping and Desalination," *J. Phys. Chem. Lett.*, vol. 8, no. 13, pp. 2842–2848, 2017.

[10] Z. Siwy and A. Fuliński, "Fabrication of a Synthetic Nanopore Ion Pump," *Phys. Rev. Lett.*, vol. 89, no. 19, pp. 4–7, 2002.

[11] A. Siria, M. L. Bocquet, and L. Bocquet, "New avenues for the large-scale harvesting of blue energy," *Nat. Rev. Chem.*, vol. 1, no. 11, 2017.

[12] N. Y. Yip and M. Elimelech, "Thermodynamic and energy efficiency analysis of power generation from natural salinity gradients by pressure retarded osmosis," *Environ. Sci. Technol.*, vol. 46, no. 9, pp. 5230–5239, 2012.

[13] B. E. Logan and M. Elimelech, "Membrane-based processes for sustainable power generation using water," *Nature*, vol. 488, no. 7411. pp. 313–319, 16-Aug-2012.

[14] G. Z. Ramon, B. J. Feinberg, and E. M. V. Hoek, "Membrane-based production of salinity-gradient power," *Energy Environ. Sci.*, vol. 4, no. 11, pp. 4423–4434, 2011.

[15] C. Y. Lin, T. Ma, Z. S. Siwy, S. Balme, and J. P. Hsu, "Tunable Current Rectification and Selectivity Demonstrated in Nanofluidic Diodes through Kinetic Functionalization," *J. Phys. Chem. Lett.*, vol. 11, no. 1, pp. 60–66, Jan. 2020.

[16] F. Chang, C. Chen, X. Xie, L. Chen, M. Li, and Z. Zhu, "A bidirection-adjustable ionic current rectification system based on a biconical micro-channel," *Chem. Commun.*, vol. 51, no. 83, pp. 15316–15319, Aug. 2015.

[17] X. He, K. Zhang, T. Li, Y. Jiang, P. Yu, and L. Mao, "Micrometer-scale ion current rectification at polyelectrolyte brush-modified micropipets," *J. Am. Chem. Soc.*, vol. 139, no. 4, pp. 1396–1399, Feb. 2017.

[18] E. B. Kalman, O. Sudre, I. Vlassiouk, and Z. S. Siwy, "Control of ionic transport through gated single conical nanopores," *Anal. Bioanal. Chem.*, vol. 394, no. 2, pp. 413–419, 2009.

[19] X. Hou, "Smart Gating Multi-Scale Pore/Channel-Based Membranes," *Adv. Mater.*, vol. 28, no. 33, pp. 7049–7064, 2016.

[20] K. B. Oldham, J. C. Myland, and A. M. Bond, *Electrochemical Science and Technology: Fundamentals and Applications*. 2011.

[21] E. Gongadze, S. Petersen, U. Beck, and U. Van Rienen, "Classical Models of the Interface between an Electrode and an Electrolyte," 2009.

[22] C. Y. Lin, L. H. Yeh, and Z. S. Siwy, "Voltage-Induced Modulation of Ionic Concentrations and Ion Current Rectification in Mesopores with Highly Charged Pore Walls," *J. Phys. Chem. Lett.*, vol. 9, no. 2, pp. 393–398, Jan. 2018.

[23] R. M. M. Smeets, U. F. Keyser, D. Krapf, M. Wu, N. H. Dekker, and C. Dekker, "Salt Dependence of Ion Transport and DNA Translocation through Solid-State Nanopores," 2006.

[24] H. S. Harned and R. L. Nuttall, "The Diffusion Coefficient of Potassium Chloride in Dilute Aqueous Solution," *J. Am. Chem. Soc.*, vol. 69, no. 4, pp. 736–740, 1947.

[25] V. M. M. Lobo, A. C. F. Ribeiro, and L. M. P. Verissimo, "Diffusion coefficients in aqueous solutions of potassium chloride at high and low concentrations," *J. Mol. Liq.*, vol. 78, no. 1–2, pp. 139–149, 1998.

[26] S. N. Inamdar, M. A. Bhat, and S. K. Haram, "Construction of Ag/AgCl reference electrode from used felt-tipped pen barrel for undergraduate laboratory," *J. Chem. Educ.*, vol. 86, no. 3, pp. 355–356, 2009.

[27] M. Taghipoor, A. Bertsch, and P. Renaud, "An improved model for predicting electrical conductance in nanochannels," *Phys. Chem. Chem. Phys.*, vol. 17, no. 6, pp. 4160–4167, 2015.

[28] M. H. Lee *et al.*, "Leakage current in a Si-based nanopore structure and its influence on noise characteristics," *Microfluid. Nanofluidics*, vol. 16, no. 1–2, pp. 123–130, 2014.

[29] J. Su *et al.*, "Anomalous Pore-Density Dependence in Nanofluidic Osmotic Power Generation," *Chinese J. Chem.*, vol. 36, no. 5, pp. 417–420, 2018.

[30] Z. Shi and J. Lipkowski, "Chloride adsorption at the Au(111) electrode surface," *J. Electroanal. Chem.*, vol. 403, no. 1–2, pp. 225–239, 1996.

[31] S. Marion, M. Macha, S. J. Davis, A. Chernev, and A. Radenovic, "Wetting of nanopores probed with pressure," pp. 1–13, 2019.

8. Appendix

8.1. Supplementary Figures

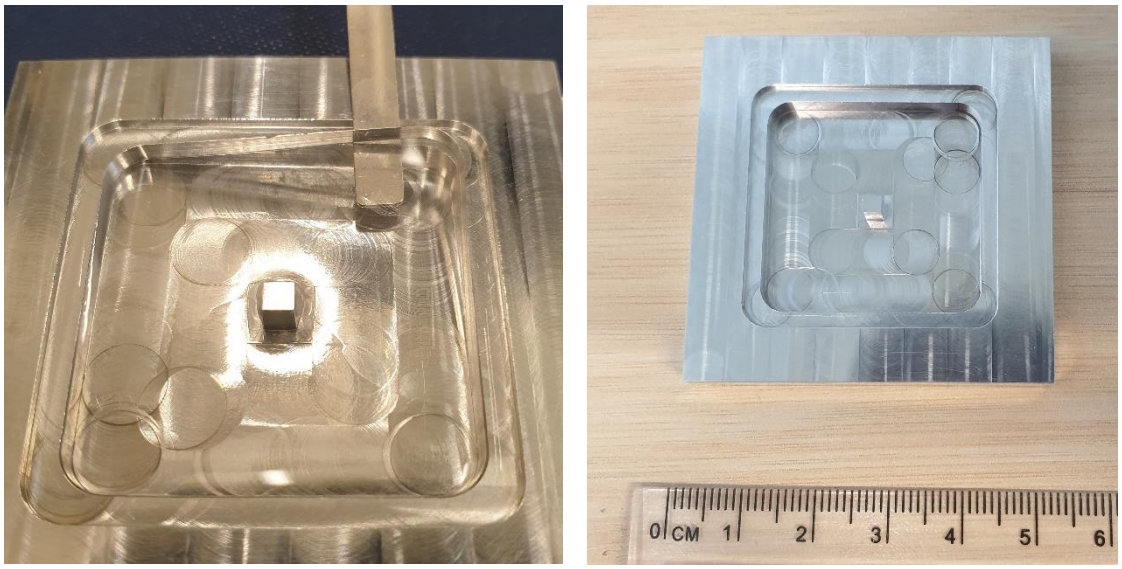

Figure 21: Aluminum mould used to cast the PDMS gaskets for the measurement setup. The PDMS is visible on the left picture, lifted by a spatula.

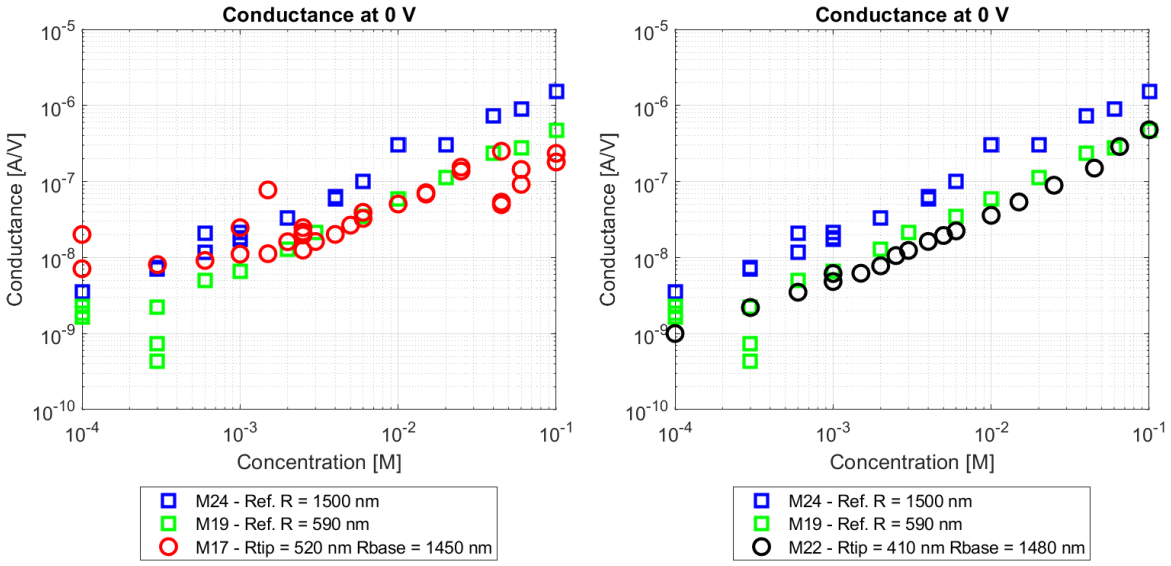

Figure 22: Differential conductance at 0 V of the two tapered channels, M17 and M22, compared to the reference channels M19 and M24.

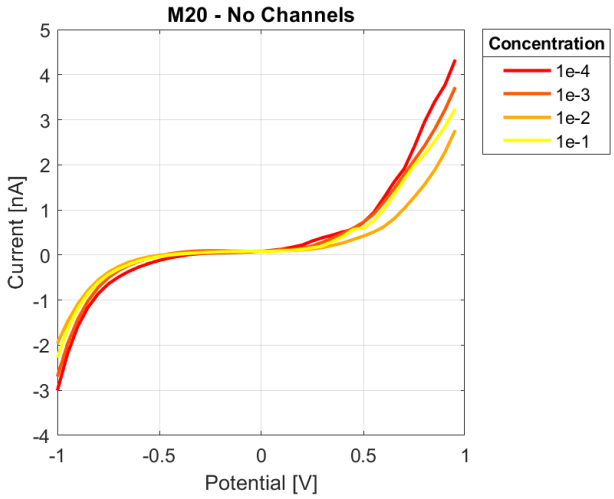

Figure 23: IV curves of the SCV measurements done on the fresh membrane at 4 different concentrations.

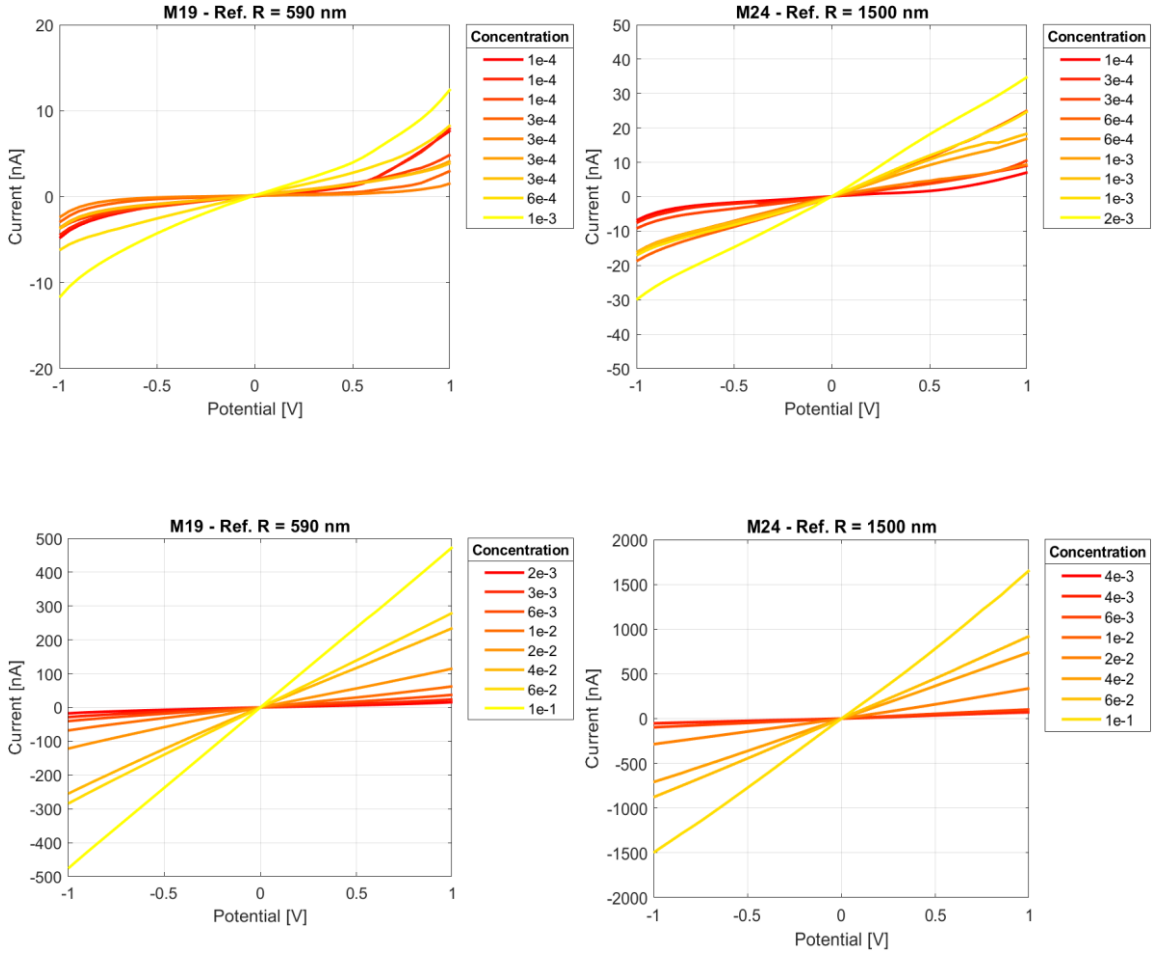

Figure 24: Non-normalized IV curves measured on the two reference channels M19 and M24. The S shape at the lowest concentrations is clearly visible.

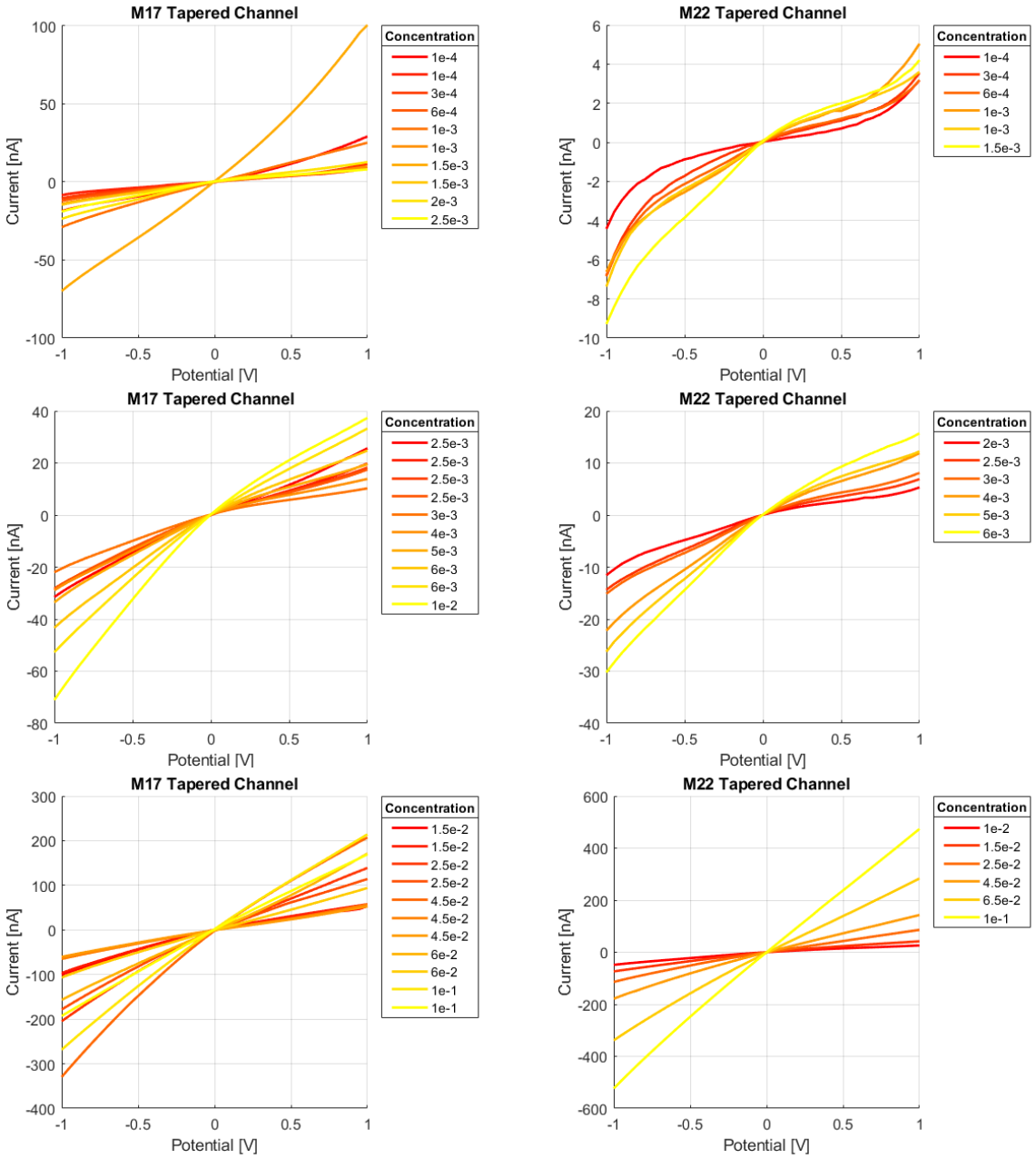

Figure 25: Non-normalized IV curves measured on the two tapered channels M17 and M22.

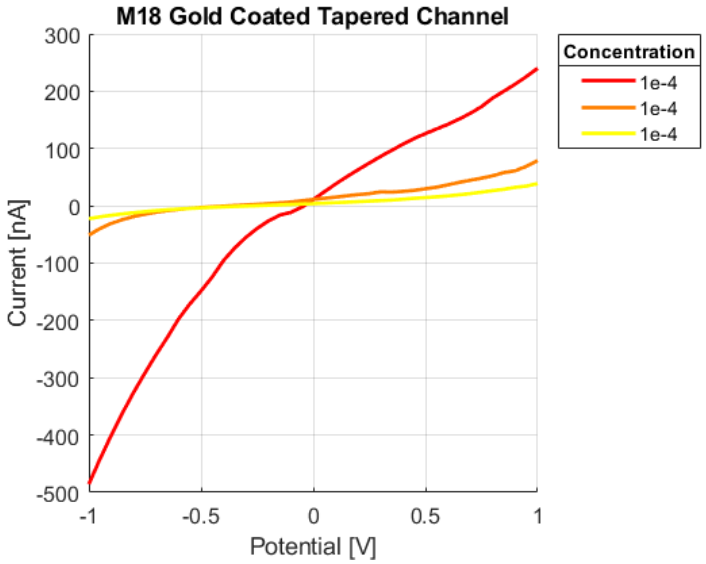

Figure 28: IV measured on the gold coated tapered channel M18. The three measurements have been done consecutively on the same solution.

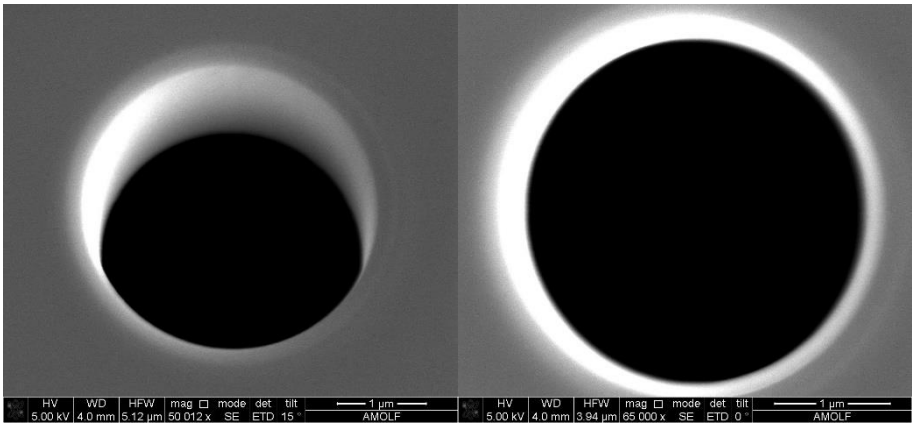

Figure 27: SEM images of the straight channel M24 right after its fabrication.

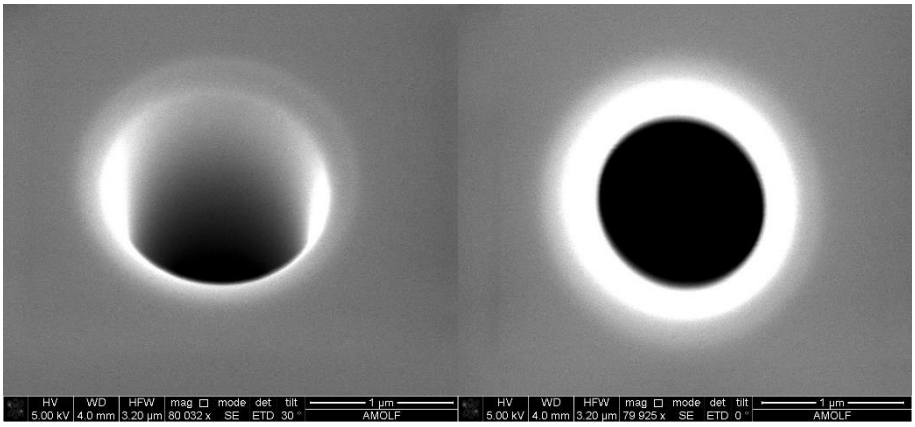

Figure 26: SEM images of the straight channel M19 right after its fabrication.

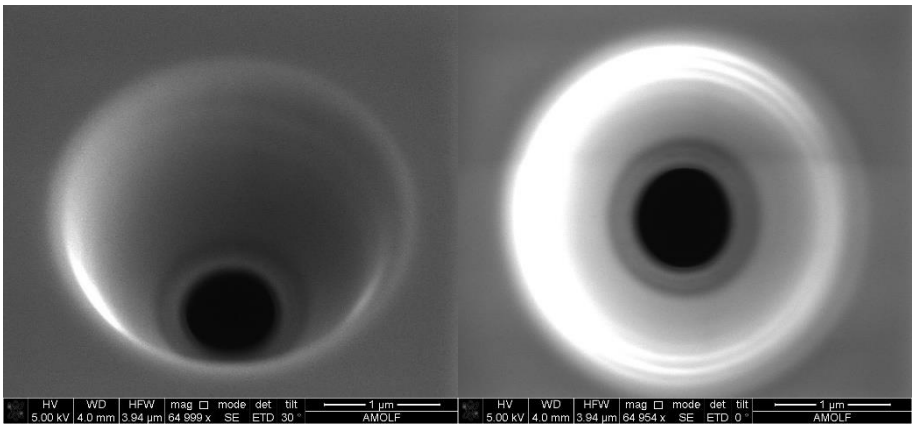

Figure 29: SEM images of the tapered channel M22 right after its fabrication.

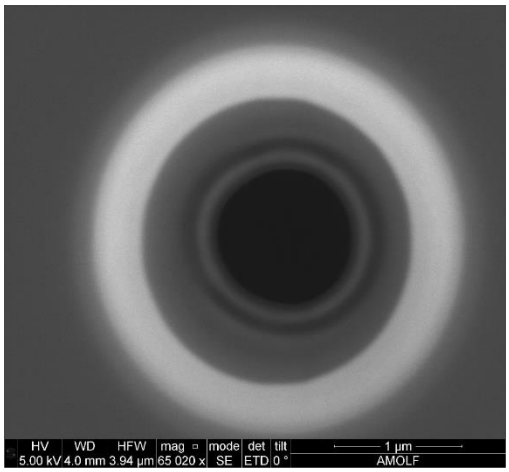

Figure 30: SEM image in top view of the tapered channel M17 right after its fabrication.

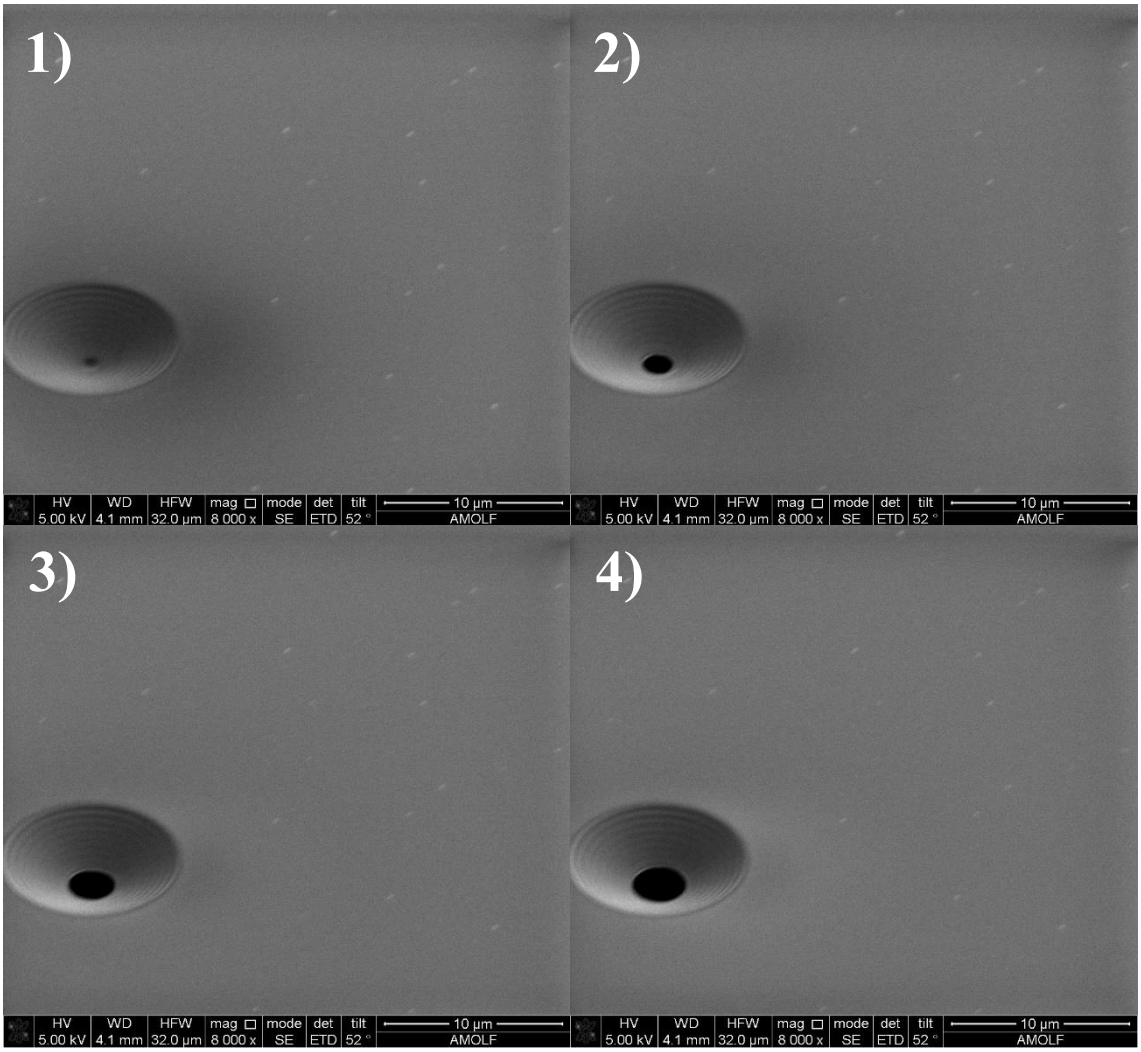

Figure 31: Example of the evolution of the channel geometry during the fabrication using the focused ion beam. The angle between the electron beam of the SEM and the ion beam of the FIB being 52°, the complete visibility on the channel is only possible for large geometries.